

# EUSPEN

Dehaeze Thomas

November 20, 2020

## Contents

<b>1</b>	<b>Tutorial: Design concepts for sub-micrometer positioning</b>	<b>@huub_janssen</b>	<b>3</b>
1.1	Positioning Terminology . . . . .		3
1.2	Principles of accuracy . . . . .		4
1.3	Case 1 - Estimate the virtual play . . . . .		5
1.4	Conventional elements for constraining DoFs . . . . .		6
1.5	Compliant elements for constraining DoFs . . . . .		6
1.6	Thin plate design . . . . .		15
<b>2</b>	<b>Keynote: Mechatronic challenges in optical lithography</b>	<b>@hans_butler</b>	<b>18</b>
2.1	Introduction . . . . .		18
2.2	Chip manufacturing loop . . . . .		18
2.3	Imaging process - Basics . . . . .		18
2.4	From stepper to scanner . . . . .		19
2.5	Dual stage scanners . . . . .		19
2.6	Immersion technology . . . . .		21
2.7	Multiple Patterning . . . . .		21
2.8	Machine layout . . . . .		22
2.9	EUV Lithography . . . . .		22
2.10	The future: high-NA EUV . . . . .		24
2.11	Challenges for future Optical Lithography machines . . . . .		24
2.12	Conclusion . . . . .		24
<b>3</b>	<b>Designing anti-aliasing-filters for control loops of mechatronic systems regarding the rejection of aliased resonances</b>	<b>@ulrich_schonhoff</b>	<b>24</b>
3.1	The phenomenon of aliasing of resonances . . . . .		24
3.2	Nature, Modelling and Mitigation of potentially aliasing resonances . . . . .		27
3.3	Anti aliasing filter design . . . . .		27
3.4	Conclusion . . . . .		33
<b>4</b>	<b>Flexure positioning stage based on delta technology for high precision and dynamic industrial machining applications</b>	<b>@mikael_bianchi</b>	<b>34</b>
4.1	Introduction . . . . .		34
4.2	Design . . . . .		34
4.3	Results . . . . .		37
4.4	Conclusion . . . . .		38
<b>5</b>	<b>Multivariable performance analysis of position-controlled payloads with flexible eigenmodes</b>	<b>@luca_mettenleiter</b>	<b>40</b>
5.1	Motivation . . . . .		40
5.2	Performance analysis with different sensitivity functions . . . . .		40
5.3	Example system . . . . .		42
5.4	Conclusion . . . . .		42

<b>6</b>	<b>High-precision motion system design by topology optimization considering additive manufacturing</b>	<b>@arnoud_delissen</b>	<b>43</b>
6.1	Introduction . . . . .		43
6.2	Case . . . . .		43
6.3	Manufacturing process . . . . .		45
6.4	Topology optimization . . . . .		45
6.5	Performance Comparison . . . . .		45
6.6	Conclusion . . . . .		45
<b>7</b>	<b>A multivariable experiment design framework for accurate FRF identification of complex systems</b>	<b>@nic_dirkx</b>	<b>47</b>
7.1	Introduction . . . . .		47
7.2	Role of directions and constrains in multivariable excitation design . . . . .		48
7.3	Solving the optimization problem . . . . .		48
7.4	Experimental validation . . . . .		50
7.5	Conclusion . . . . .		50
<b>8</b>	<b>Keynote: High precision mechatronic approaches for advanced nanopositioning and nanomeasuring technologies</b>	<b>@eberhard_manske</b>	<b>51</b>
8.1	Coordinate Measurement Machines (CMM) . . . . .		51
8.2	Difference between CMM and nano-CMM . . . . .		51
8.3	How to do nano-CMM . . . . .		51
8.4	Concept - Minimization of the Abbe Error . . . . .		52
8.5	Minimization of residual Abbe error . . . . .		52
8.6	Compare of long travel guiding systems . . . . .		52
8.7	Extended 6 DoF Abbe comparator principle . . . . .		54
8.8	Practical Realisation . . . . .		54
8.9	Tilt Compensation . . . . .		55
8.10	Comparison of long travail guiding systems - Bis . . . . .		56
8.11	Drive concept . . . . .		56
8.12	NPMM-200 with extended measuring volume . . . . .		56
8.13	measurement capability . . . . .		57
8.14	Extension of the measuring range (700mm) . . . . .		57
8.15	Inverse kinematic concept - Tetrahedral concept . . . . .		57
8.16	Inverse kinematic concept - Scanning probe principle . . . . .		60
8.17	Inverse kinematic concept - Compact measuring head . . . . .		61
8.18	Inverse kinematic concept - Scanning probe principle . . . . .		61
8.19	Conclusion . . . . .		61
<b>9</b>	<b>Reducing control delay times to enhance dynamic stiffness of magnetic bearings</b>	<b>@jan_philipp_schmidtmann</b>	<b>63</b>
9.1	Introduction . . . . .		63
9.2	Time Delay Reduction . . . . .		63
9.3	Practical Realization . . . . .		65
9.4	Results . . . . .		65
9.5	Conclusion . . . . .		65
<b>10</b>	<b>Digital twins in control: From fault detection to predictive maintenance in precision mechatronics</b>	<b>@koen_classens</b>	<b>66</b>
10.1	Motivation . . . . .		66
10.2	Predictive Maintenance . . . . .		66
10.3	Objectives . . . . .		69
10.4	Null-space based FDI . . . . .		69
10.5	Roadmap from fault detection to predictive maintenance . . . . .		71

# 1 Tutorial: Design concepts for sub-micrometer positioning

@huub\_janssen

## 1.1 Positioning Terminology

- **Accuracy:** Accuracy describes how close the mean result is to the reference value. (Figure 1)
- **Repeatability:** Repeatability describes the variation between results. (Figure 1)
- **Resolution:** The resolution of a system is equal to the smallest incremental step that can be made (Figure 2)
- **Stability:** The stability of a system is the maximum deviation from a constant reference value over time. The stability is always related to the time frame taken into account. (Figure 3)

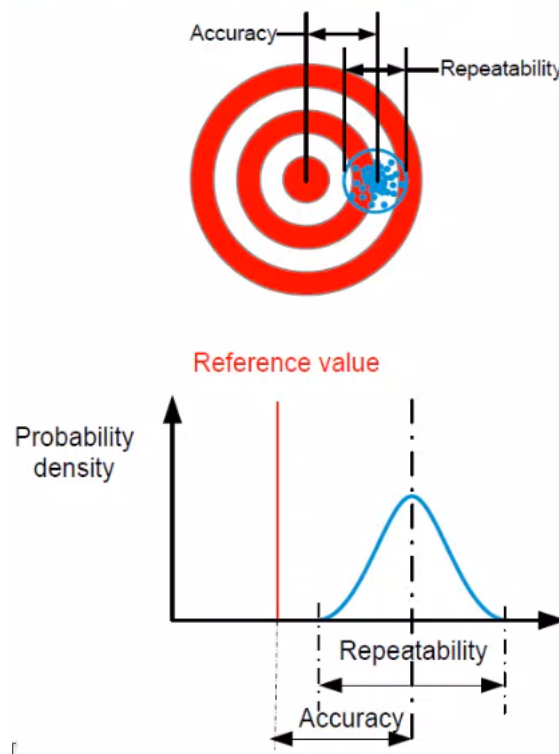


Figure 1: Accuracy and Repeatability

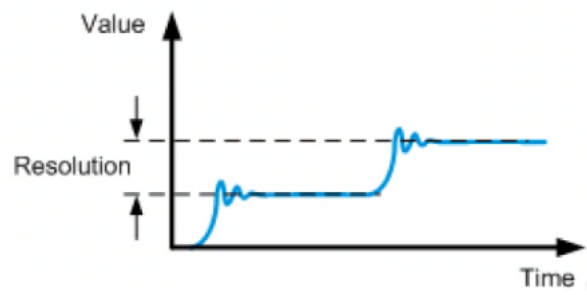


Figure 2: Position Resolution

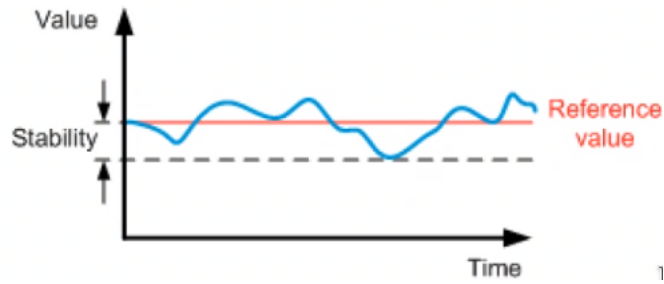


Figure 3: Position Stability

## 1.2 Principles of accuracy

Limited stiffness, play and friction will induce an hysteresis for a positioning system as shown in Figure 4. The hysteresis can actually help estimating the play and friction present in the system.

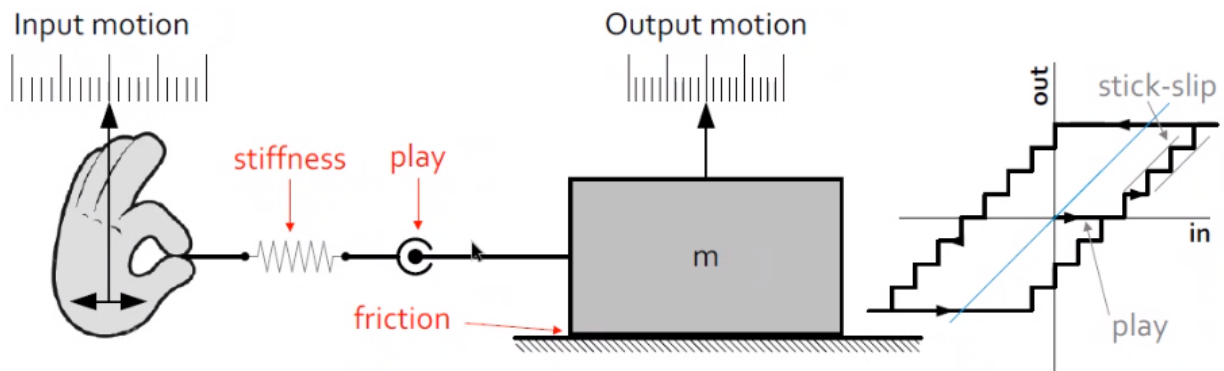


Figure 4: Stiffness, play and Friction

Ways to make the hysteresis smaller:

- avoid play (=> use compliant elements)
- minimize friction
- use high stiffness

The position uncertainty of a system can be estimated as follow (Figure 5):

$$\text{Position Uncertainty} = \text{play} + 2 \times \text{Virtual Play} \quad (1)$$

where the virtual play can be estimated as follow:

$$\text{Virtual Play} = \frac{\text{Friction Force}}{\text{Actuator Stiffness}} = \frac{F_w}{c} \quad (2)$$

When considering dynamics, the goal is to make the first resonance frequency much higher than the frequency of the wanted motion. Thus, the general recommendation is then to minimize mass and to increase stiffness.

Moreover, we generally want things to be predictable:

- constant, preferably no friction. Note that it is very difficult to make a system with constant friction in practice, so better make a system with no friction.

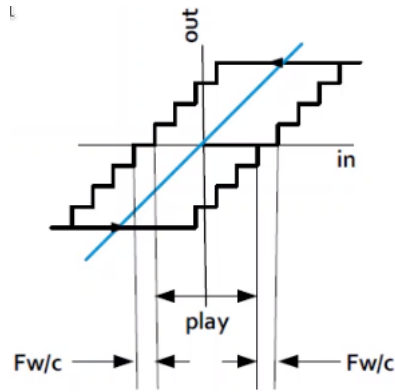


Figure 5: Hysterestis, play and virtual play

- no play
- high stiffness
- low pass

### 1.3 Case 1 - Estimate the virtual play

Estimate the virtual play of the system in Figure 6 with following characteristics:

- Payload:  $m = 20 \text{ kg}$
- Friction coefficient in drive direction:  $f = 0.05$
- Table stroke:  $L = 300 \text{ mm}$
- Screw spindle inner diameter:  $d = 8 \text{ mm}$
- Spindle Material: Stainless steel

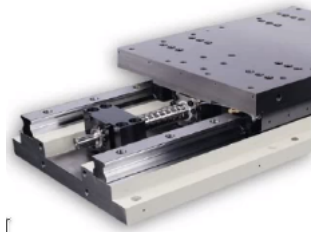


Figure 6: Studied system for “Case 1”

First the friction force can be calculated as the vertical mass times the friction coefficient:

$$F_w = (mg)f \quad (3)$$

Then, the axial stiffness of the screw spindle is computed:

$$c = \frac{A}{L}E \quad (4)$$

with:

- $A = \pi d^2$  is the screw section area
- $L = 300 \text{ mm}$  is the screw length

- $E$  is the Young modulus of stainless steel

And finally:

$$\text{Virtual Play} = \frac{F_w}{c} \approx 0.6 \mu m \quad (5)$$

## 1.4 Conventional elements for constraining DoFs

There exist many conventional elements for constraining DoFs. Some of them are:

- Struts with ball joint: 1DoF constrained (Figure 7)
- Ball bearing: 5DoF constrained (Figure 8)
- Guide with roller bearing: 4DoF constrained (Figure 9)
- Roller rail guide: 5DoF constrained (Figure 10)



Figure 7: Ball Joint



Figure 8: Ball Bearing



Figure 9: Roller Bearing

## 1.5 Compliant elements for constraining DoFs

### 1.5.1 Basic leaf springs and folded leaf springs

An example of a compliant element is shown in Figure 11.

Other types of compliant elements include:

- Leaf spring: constrains 3 dof (Figure 12)
- Folded leaf spring: constrains only 1dof (Figure 13) These are generally used in combination with other folded leaf springs.
- Flexure pivots: constrains 5 dofs (Figure 14)

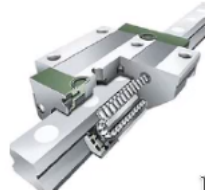


Figure 10: Roller Rail Guide



Figure 11: Example of 1dof constrained compliant element

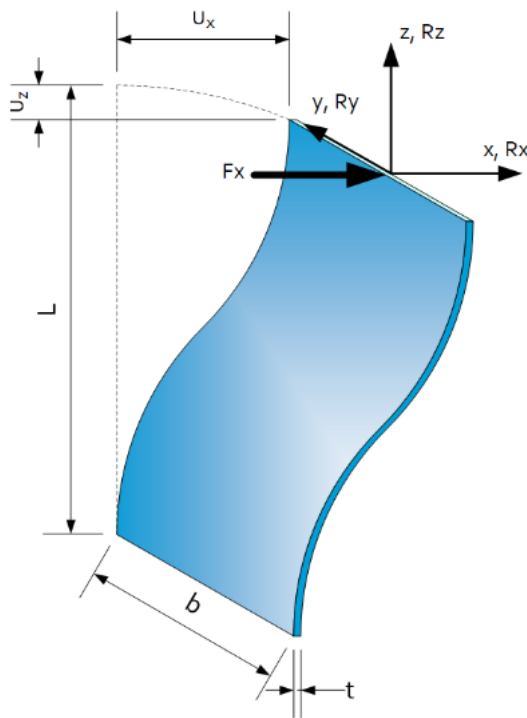


Figure 12: Leaf springs

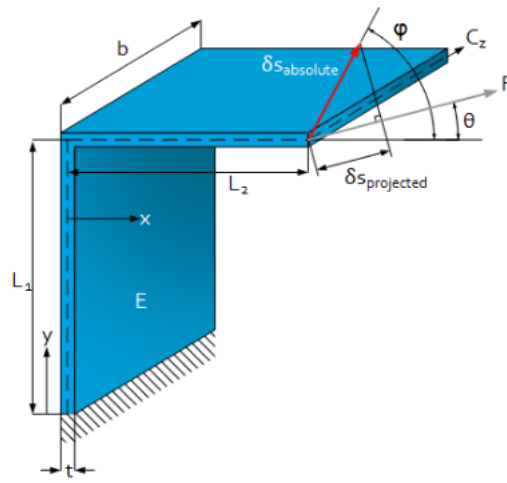


Figure 13: Folded Leaf springs

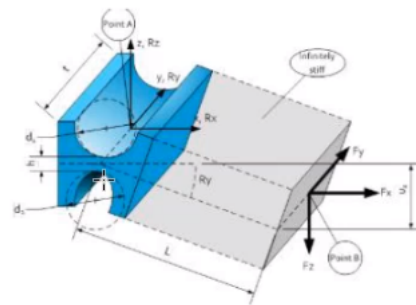


Figure 14: Flexure Pivots (5dof constrained)



### 1.5.2 1dof Parallel Guiding

Parallel guiding can be made using two leaf springs (Figure 15):

- 2 parallel leaf springs
- Force actuator in center of parallelism (middle of the leaf springs) to avoid coupled rotation
- Sag in vertical direction as a function as the horizontal displacement. This sag is predictable and reproducible:

$$\delta z = 0.6 \frac{x^2}{L} \quad (6)$$

- Vertical stiffness negatively affected by displacement
- Take care of maximum buckling (Figure 16)
- Improve buckling load and Z stiffness by reinforced mid-section (Figure 17)

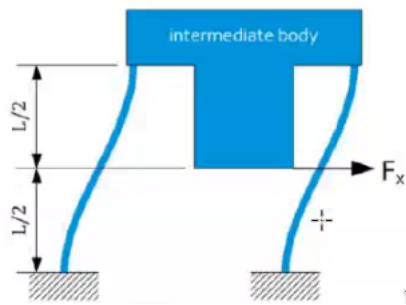


Figure 15: Parallel guiding

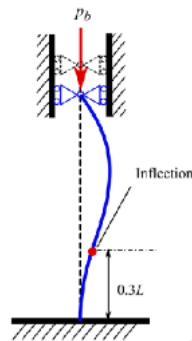


Figure 16: Example of bucklink

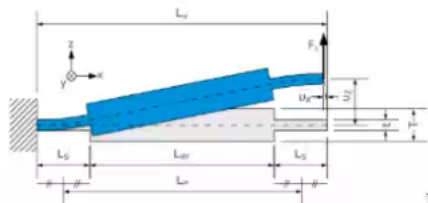


Figure 17: Reinforced leaf springs

### 1.5.3 Rotation Compliant Mechanism

Figure 18 shows a rotation compliant mechanism:

- 3 leaf springs
- no sensitive for thermal load on the body: as the central part heat ups and expand, the center line of the rotation stays at the same position

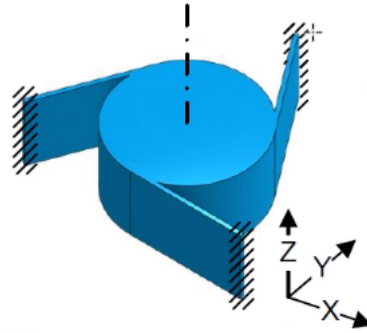


Figure 18: Example of rotation stage using leaf springs

### 1.5.4 Z translation

Figure 19 shows a Z translation mechanism:

- 5 struts (“needles”)
- Not sensitive for thermal loads on body

The problem is that when it moves vertical, there will also be some z rotation because the length of the strut is fixed (stiff). This parasitic rotation is however predictable.

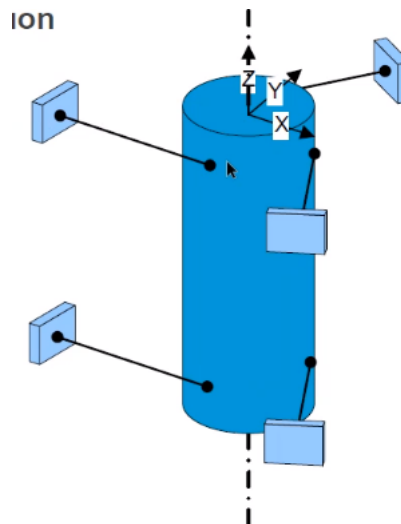


Figure 19: Z translation using 5 struts

An alternative is to use folder leaf springs (Figure 20), and this avoid the parasitic rotation.

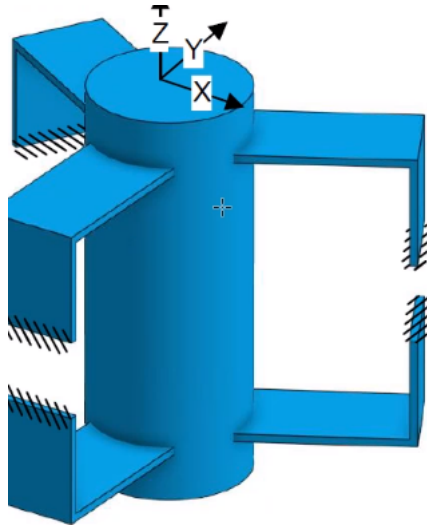


Figure 20: Z translation using 5 folded leaf springs

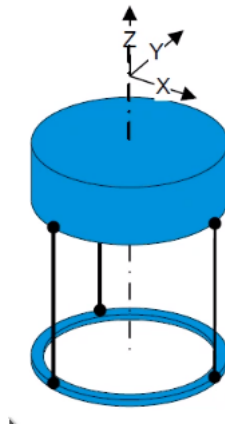


Figure 21: X,Y,Rz using 3 struts

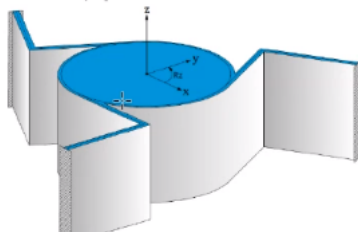


Figure 22: X,Y,Rz using 3 folded leaf springs

### 1.5.5 X-Y-Rz Stage

An X-Y-Rz stage can be done either using 3 struts (Figure 21) or using 3 folded leaf springs (Figure 22).

### 1.5.6 Compliant mechanism with only one fixed dof

The compliant mechanism shown in Figure 23 only constrain the rotation about the y-axis.

◆ Which degree(s) of freedom fixed?

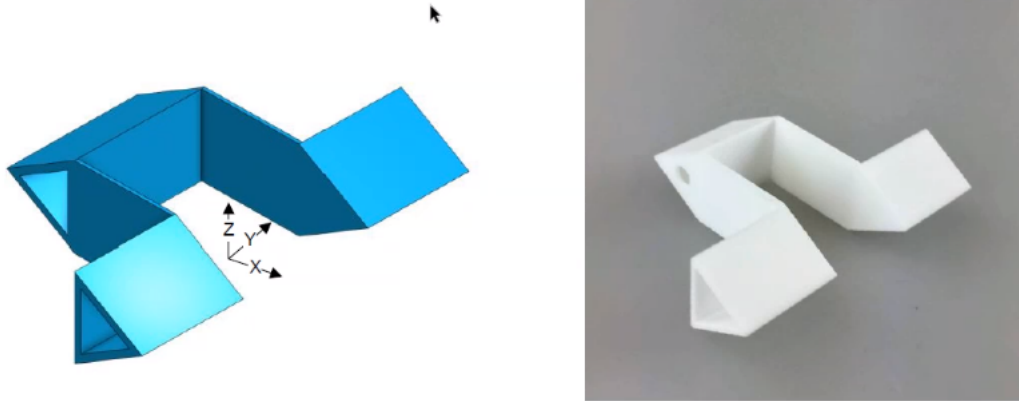


Figure 23: 5dof motion, only the  $R_y$  is constrained

### 1.5.7 Summary

- compliant elements enable defined movements
- Hinges or guidings can be used for small movements
- **No play, No friction, No wear, No contamination**
- **but limited rotation, need a constant force to hold in place**

### 1.5.8 Examples

An example of a complex compliant mechanism is shown in Figure 24.

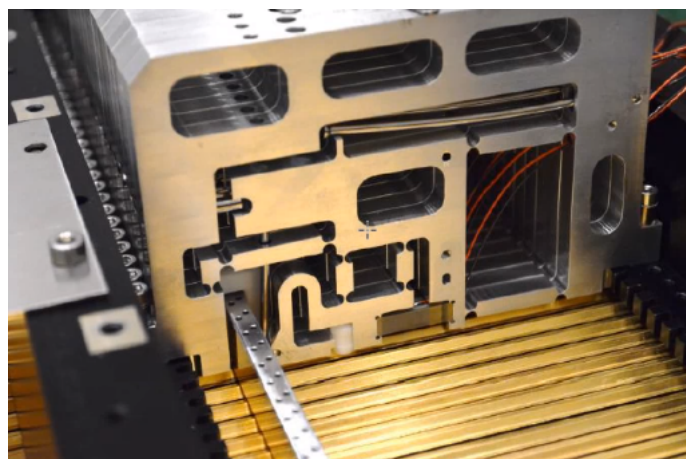


Figure 24: Design concept

Figure 25 shown a reinforced part to avoid buckling and improve vertical stiffness.



Figure 25: Use leaf springs instead of linear roller bearings

### 1.5.9 Mechatronics positioning challenge

A X-Y-Rz stage is shown in Figure 26. To make this stage usable for nano-metric positioning, the following ideas were used:

- Use parallel mechanisms instead of serial one:
  - no stacking of errors
  - smaller, stiffer, in one plane
- Symmetry:
  - Use 3 identical voice coil actuators
  - Use 3 identical sensors
  - Center position insensitive for temperature change
- Flexure only;
  - no friction
  - no play
  - no wear
  - no particulate (important for clean rooms)
  - no service
- Continuously under control:
  - no alignment / crosstalk issues between axes
  - voice coil / sensors combination determines performance

<https://www.youtube.com/watch?v=OjNnHa6O9A8>video

### 1.5.10 Case - Play Free parallel Stage

Figure 27 shows a parallel mechanism that should be converted to a compliant mechanism. Its characteristics are:

- 1mm stroke

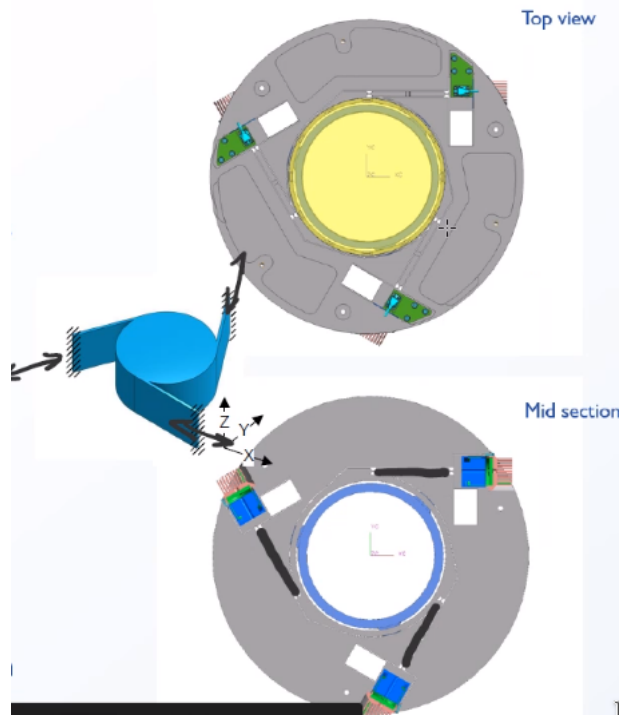


Figure 26: Example of X-Y-Rz positioning stage

- 1:5 lever arm
- 10kg payload
- distance between hinges: 5mm
- thickness  $t$ : 40mm
- Material: aluminium

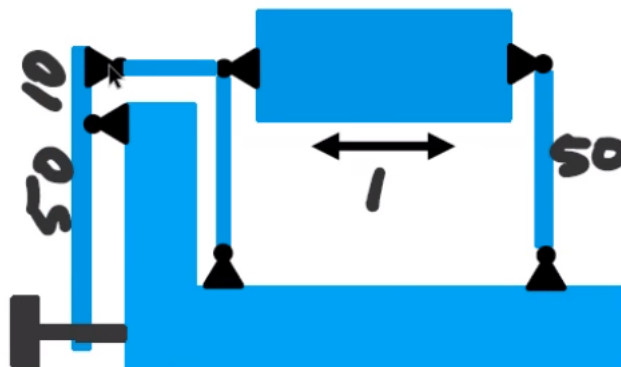


Figure 27: Example of a parallel stage that should be converting to a compliant mechanism

The goals are to:

- Make design using elastic hinges
- Maximize vertical stiffness

- Determine vertical stiffness

The solution is shown in Figure 28.

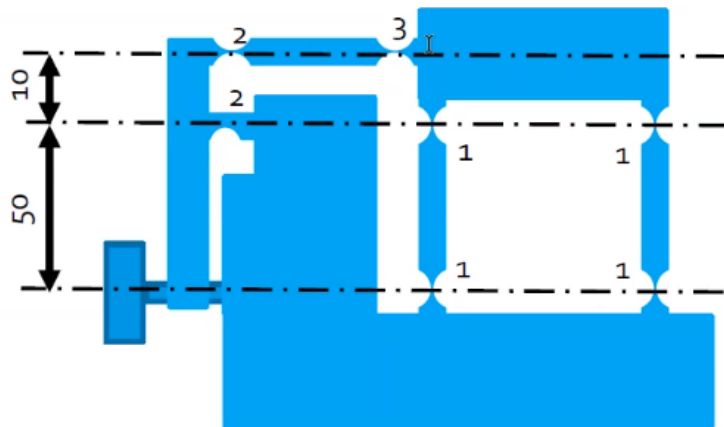
$$\sigma = 0.58E \sqrt{\frac{h}{D}} R_y = 0.58E \sqrt{\frac{h}{D}} \frac{u}{L};$$

$$E = 70 \cdot 10^3 \text{ N/mm}^2; \sigma = 460 \text{ N/mm}^2$$

Type 1:  $u=0.5 \text{ mm}$ ,  $L=10 \text{ mm}$   
 $h/D < 0.05$ ; Practical :  $h=0.3$ ,  $D=6$

Type 2:  $u=0.5 \text{ mm}$ ,  $L=50 \text{ mm}$   
 $h/D < 1.3$ ; Practical :  $h=1$ ,  $D=6$

Type 3: not critical:  $h=1$ ,  $D=6$



Vertical stiffness:  $C = 2 * 0.24Et \sqrt{\frac{h}{D}}$

$$C = 2 * 0.24 * 70 * 10^3 * 40 * \sqrt{\frac{h}{D}}$$

$$C = 6 * 10^5 \text{ N/mm} = 6 * 10^8 \text{ N/m} !$$

Figure 28: Case Solution

## 1.6 Thin plate design

### 1.6.1 Thin plate in torsion

Thin plates are very important for compliant mechanisms.

The torsion stiffness of a thin plate is linear with the length of the thin plate:

$$k = \frac{GI_p}{L} \quad (7)$$

with  $G$  the shear modulus:

$$G \approx 0.3E \quad (8)$$

where  $E$  is the young modulus

Then

$$I_p = \frac{1}{3}ht^3 = \frac{1}{3}At^2 \quad (9)$$

where  $A$  is the area of the cross section.

### 1.6.2 Difference between open and close profile

The close profile has much more torsional stiffness than the open profile.

Just by opening the tube, we have a much smaller torsional stiffness (but almost same axial stiffness for instance).

We have similar behavior with an open/closed box. If we remove one side of the cube shown in Figure 31, we would have much smaller torsional stiffness along the axis perpendicular to the removed side.

If we use triangles, we obtain high torsional stiffness as shown in Figure 32.

Frames are usually corresponding to open-boxes with have a small stiffness in torsion. On way to reinforce it is using triangles.

A nice way to have a 1dof flexure guiding with stiff frame is shown in Figure 33.

A plate under torsion (2/2)

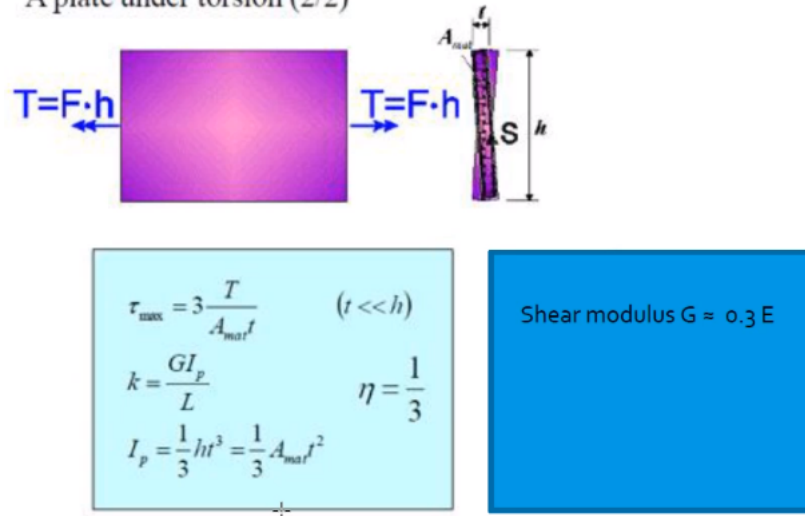


Figure 29: A plate under torsion

Stiffness comparison open- and closed tube (torsion)

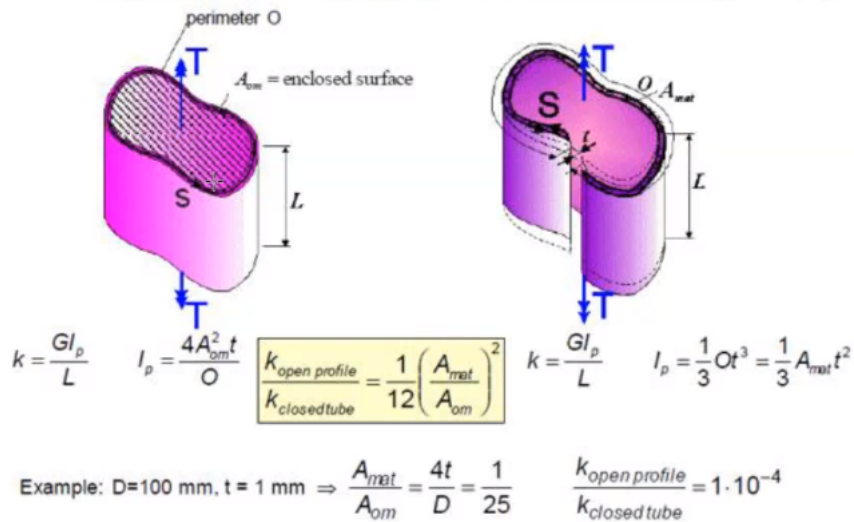


Figure 30: Stiffness comparison open and closed tube (torsion)



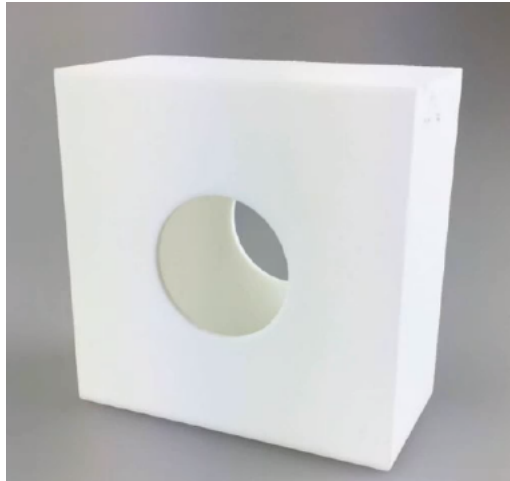


Figure 31: Closed box.

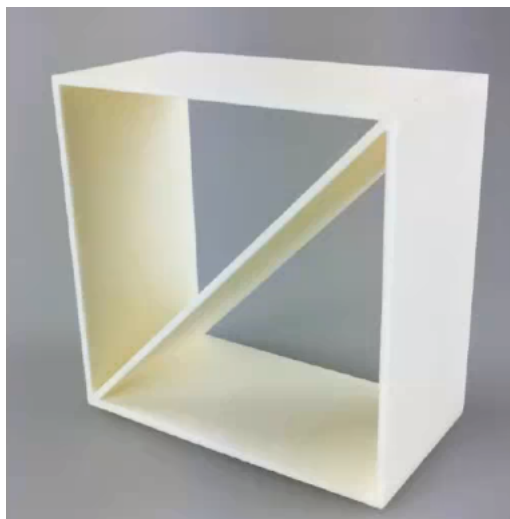


Figure 32: Open box (double triangle)



Figure 33: Box with integrated flexure guiding

## 2 Keynote: Mechatronic challenges in optical lithography @hans\_butler

### 2.1 Introduction

**Question:** in chip manufacturing, how do developments in optical lithography impact the mechatronic design?

Main developments:

- Scanning & dual stage scanning
- Immersion
- Multiple patterning
- Extreme ultra violet lithography

### 2.2 Chip manufacturing loop

In this presentation, only the exposure step is discussed (lithography).

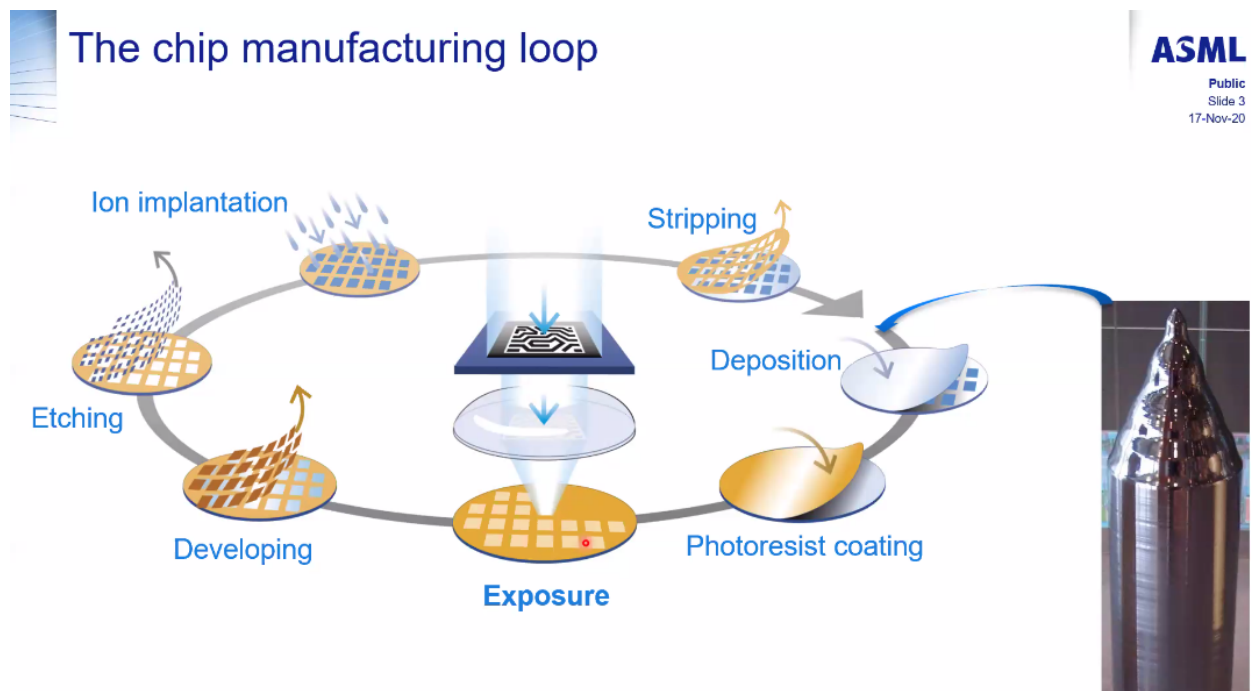


Figure 34: Chip manufacturing loop

### 2.3 Imaging process - Basics

- An illuminator provides light at constant wavelength  $\lambda$
- The pattern on the reticle diffracts the light into order
- At least  $\pm 1$ st orders need to be captured. This will induce a sinusoidal wave on the wafer as shown in Figure 35.
- Wafer and mask are placed on high accuracy moving stages

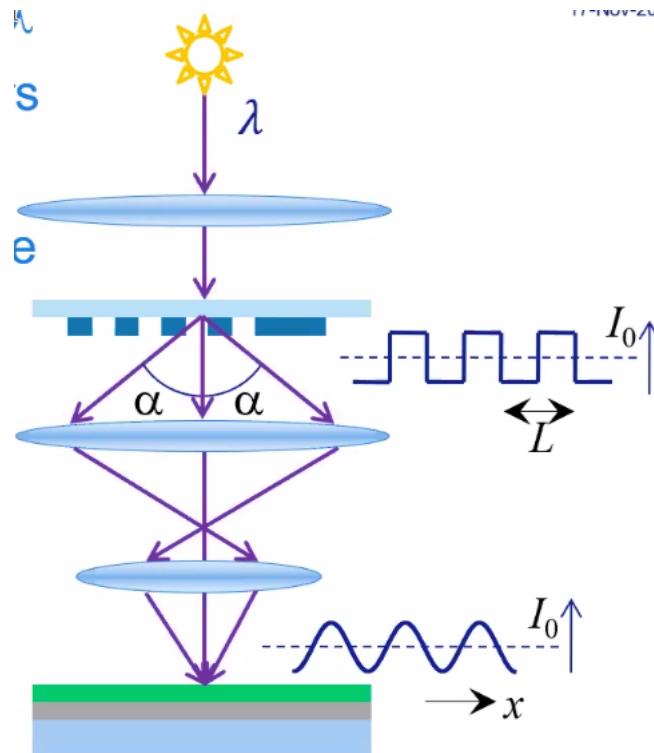


Figure 35: Imaging process - basics

## 2.4 From stepper to scanner

Before, one chip was illuminating at a time, but people wanted to make bigger chips. However, it was difficult to make larger lenses.

The solution was to use a scanner, where both the mask and wafer are on moving stages. This implied many requirements in dynamics and accuracy!

## 2.5 Dual stage scanners

Both the reticle stage and wafer stage are moving. In order to have the same throughput, higher stage accelerations are required.

This implies some mechatronics challenges:

- higher stage acceleration
- higher accuracy
- interaction between stages

Which are solved by:

- Larger forces => balance masses
- Stage dynamical design for high bandwidth control
- Control coupling between stages (one control system can act as a disturbance to another controlled system => feedforward)

Scanning provides larger fields and better imaging and focus  
Challenge: High-accuracy synchronized scanning of wafer & reticle

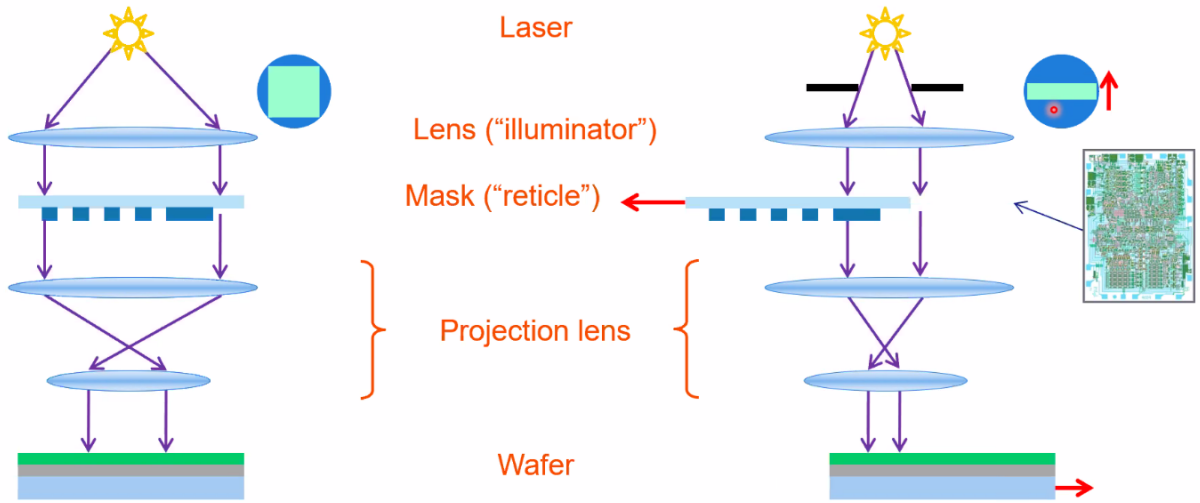


Figure 36: From stepper to scanner



Figure 37: Machine based on the dual stage scanners

## 2.6 Immersion technology

Water is used between the lens and the wafer to increase the “NA” and thus decreasing the “critical dimension”.

The “hood” is there to prevent any bubble to enter the illumination area (Figure 38). The position of the “hood” is actively control to follow the wafer stage (that can move in z direction and tilt).

Three solutions are used for the positioning control of the “hood” system (Figure 39):

- Disturbance decoupling
- Iterative learning control
- Feed-forward control from the Wafer control signal

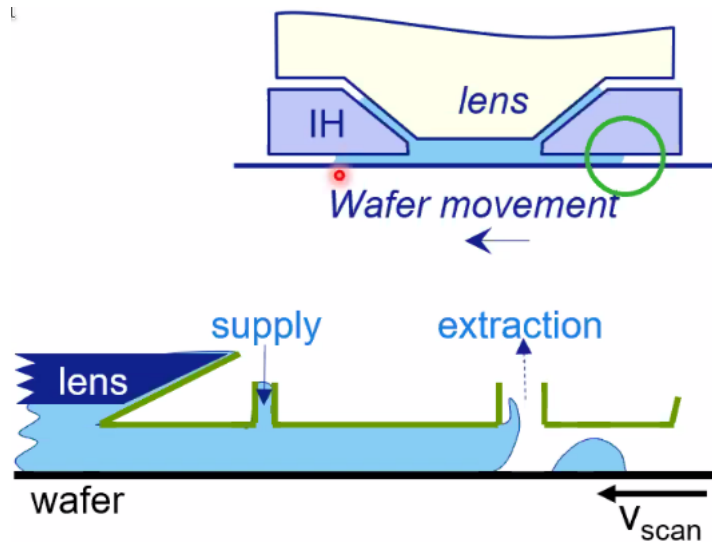


Figure 38: Hood System

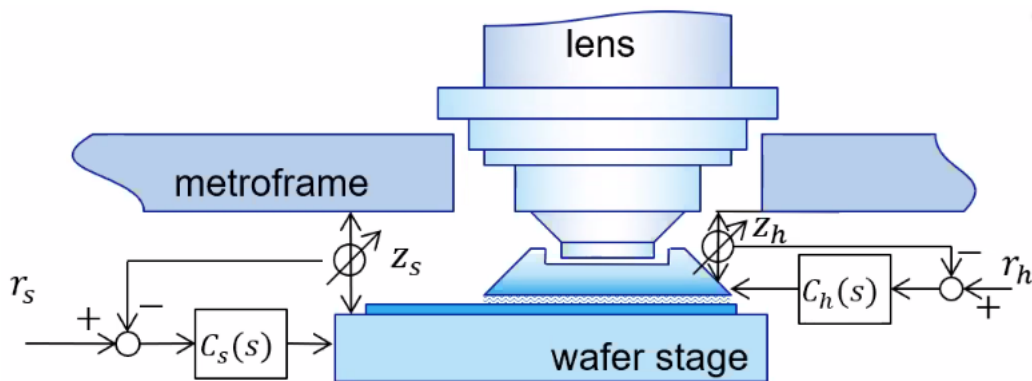


Figure 39: Control system for the “hood”

## 2.7 Multiple Patterning

The multiple patterning approach adds few mechatronics challenges:

- Position accuracy limited to  $\sim 4\text{nm}$  due to interferometer position measurement (variation of temperature/pressure of air)
- Stage swap is complex and time-consuming

This was solved by:

- Using encoder instead of interferometers
- Use long stroke motor: h-stage => new wafer stage concept

## 2.8 Machine layout

Each stage is controlled with 6dof lorentz short stroke actuators (Figure 40). The magnet stage can move horizontally (due to reaction forces of the wafer stages): it asks as a balance mass.

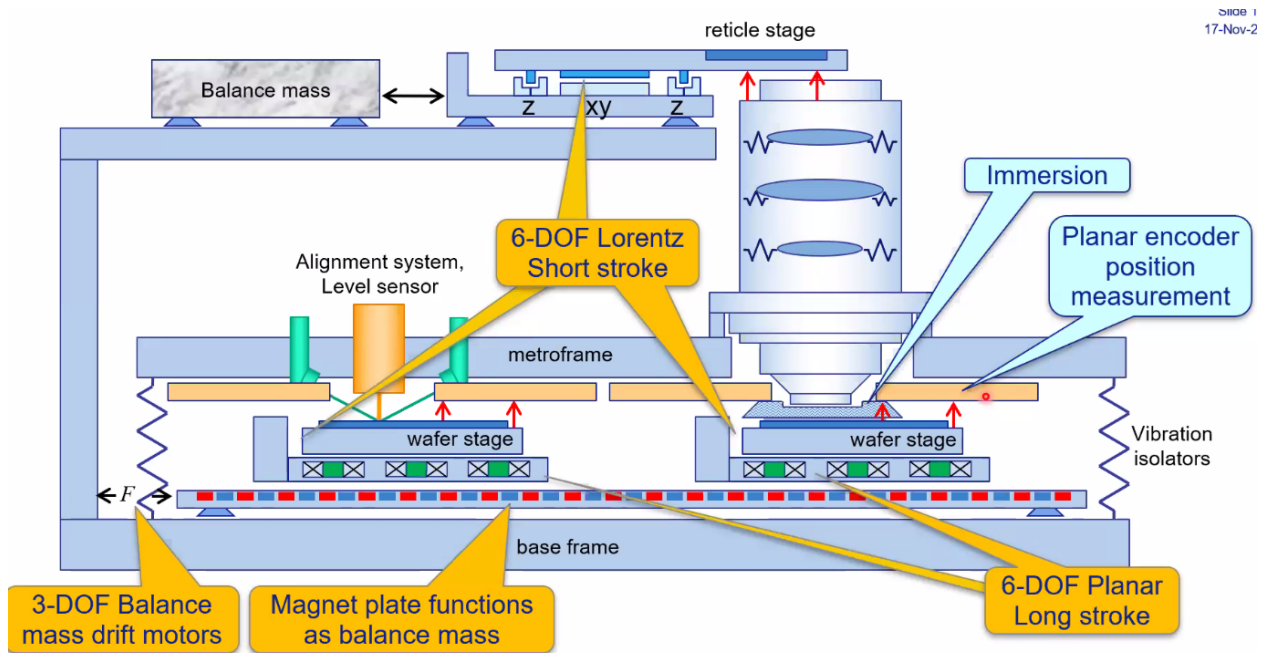


Figure 40: Machine layout

## 2.9 EUV Lithography

Vacuum is required which implies:

- no bearings
- no cooling

All the optics are reflective:

- extremely accurately polished
- challenge: keep mirrors optimally positioned

Wafer stage:

- Move at high speed and accelerations
- Challenge: in vacuum
- Solved by: mechanically suspended balance mass, and interferometer position measured can be used because it is in vacuum now

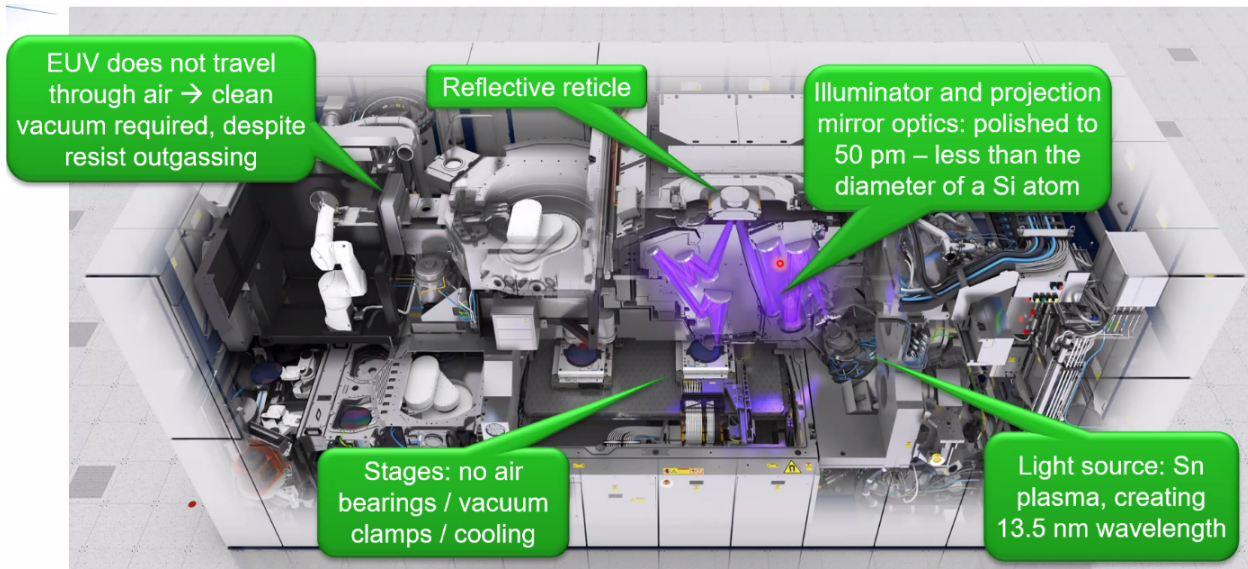


Figure 41: Schematic of the ASML EUV machine

$\lambda$ [nm]	Source	NA	CD [nm]	Intro	Type
$\geq 365$	Hg lamp	0.65	350	<1990	/4x0
248	KrF laser	0.80	110	1998	/8x0
193	ArF Laser	0.93	65	2000	/14x0
193i	ArF Laser	1.35	38	2005	/19x0
157	F <sub>2</sub> Laser	<1	?	never	/1600
13.5	Sn plasma	0.33	13	2011	/3400
13.5	Sn plasma	0.55	8	202x	/5000

Figure 42: The CD will be 8nm

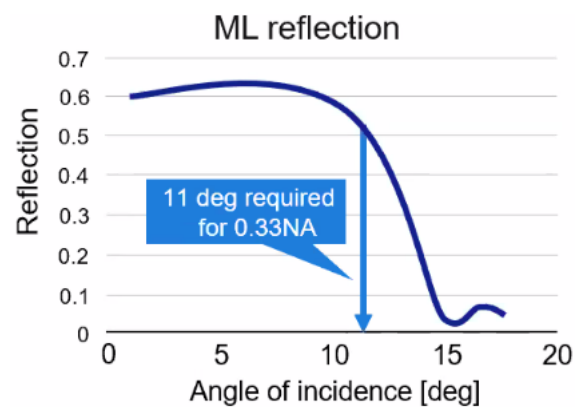


Figure 43: Change of reflection of a mirror as a function of the angle of incidence

## 2.10 The future: high-NA EUV

In order to do so, high “opening” of the optics is required which is very challenges because the reflectiveness of mirror is decreasing as high angle of incidence (Figure 43).

## 2.11 Challenges for future Optical Lithography machines

Challenges:

- Double wafer stage acceleration
- Much bigger mirrors
- Tighter accuracy specifications despite

Solutions:

- Stage and mirror dynamics, high bandwidth control
- Dynamics architecture: improved isolation, multiple isolate sets
- Heating compensation

## 2.12 Conclusion

The conclusions are:

- Lithographic tools are the main enabler for over shrinking device sizes
- New (optical) requirements lead to new mechatronic challenges:
  - Larger fields / better imaging: from stepping to scanning
  - Larger wafer size: dual stage scanners
  - Immersion: wafer stage & hood control
  - Multiple patterning: planar motors and encoder technology
  - EUV: all-vacuum stages
  - High-NA EUV: new optics, much larger accelerations

# 3 Designing anti-aliasing-filters for control loops of mechatronic systems regarding the rejection of aliased resonances @ulrich\_schonhoff

## 3.1 The phenomenon of aliasing of resonances

Weakly damped flexible modes of the mechanism can limit the performance of motion control systems.

For discrete time controlled systems, there can be an additional limitation: aliased resonances which are rarely discussed.

The aliasing of signals is well known (Figure 45).

However, aliasing in systems can also happens and is schematically shown in Figure 46.

The poles of the system will be aliased and their location will change in the complex plane as shown in Figure 47.

More precisely:

- the imaginary parts of the poles mirror about the Nyquist frequency
- the real parts of the poles remain equal

Therefore, the damping of the aliased resonances are foreseen to have larger dampings.

Let's consider two systems with a resonance:



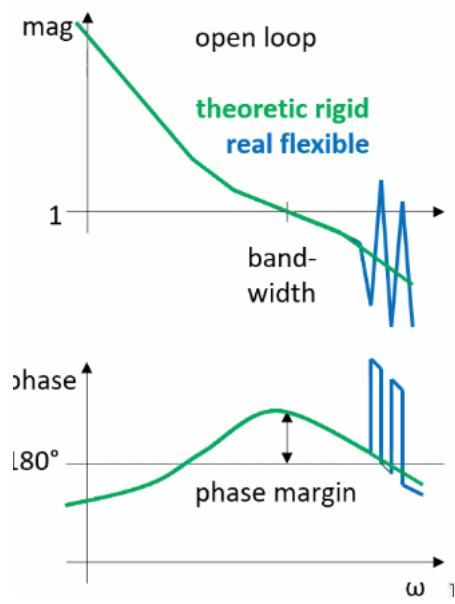


Figure 44: Example of high frequency lightly damped resonances

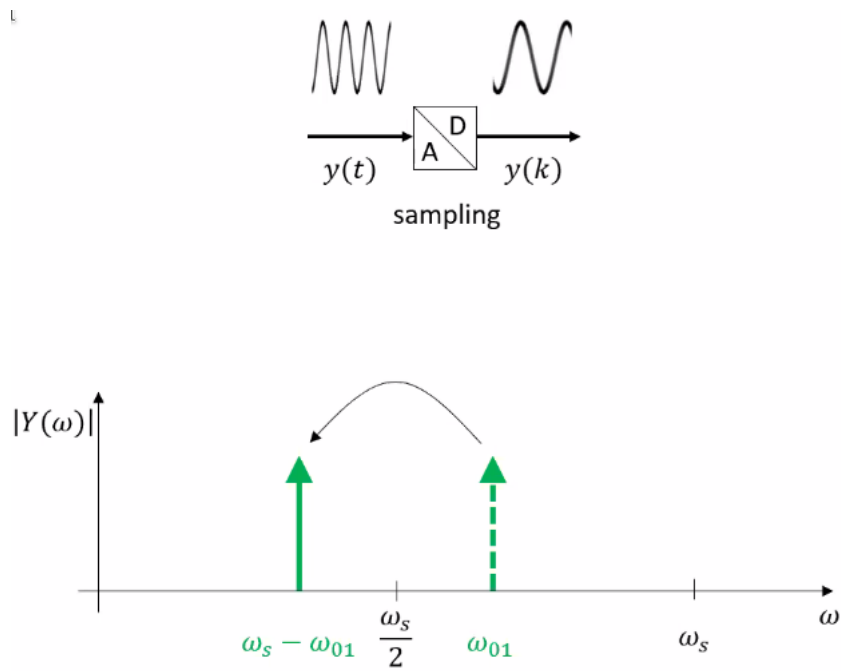


Figure 45: Aliasing of Signals

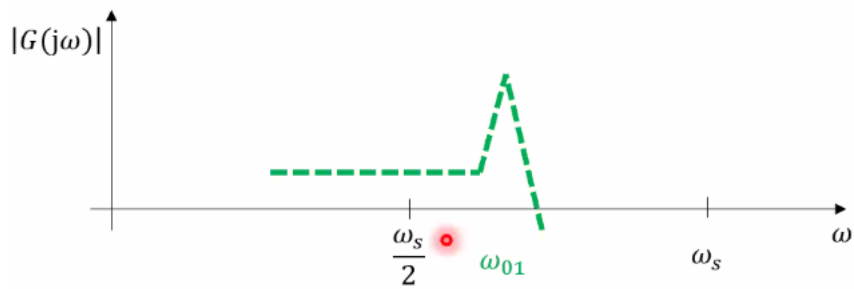
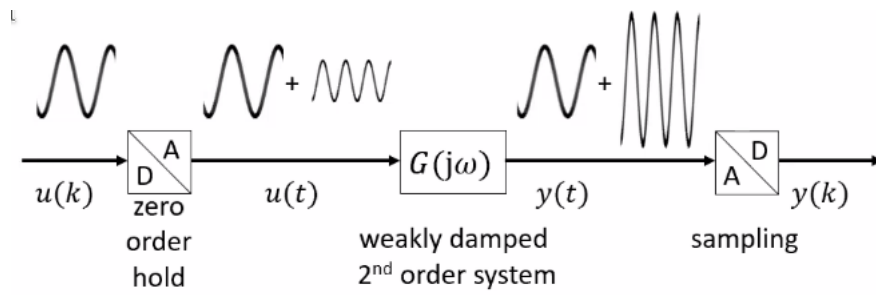


Figure 46: Aliasing of Systems

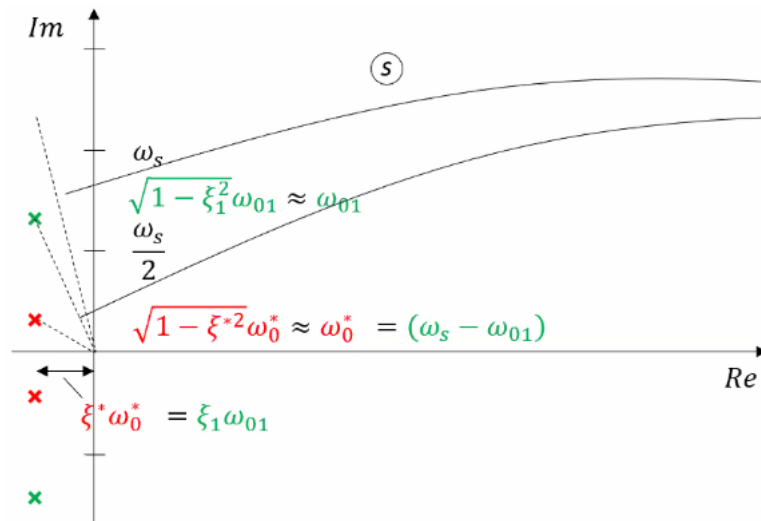


Figure 47: Aliasing of poles in the complex plane

1. below the Nyquist frequency (blue dashed)
2. above the Nyquist frequency (green dashed)

Then looking at the same systems in the digital domain, one can see that then the resonance is above the Nyquist frequency (Figure 48):

- the resonance mirrors
- the damping is increased

Therefore, when identifying a low damped resonance, it could be that it comes from a high frequency low damped resonance.

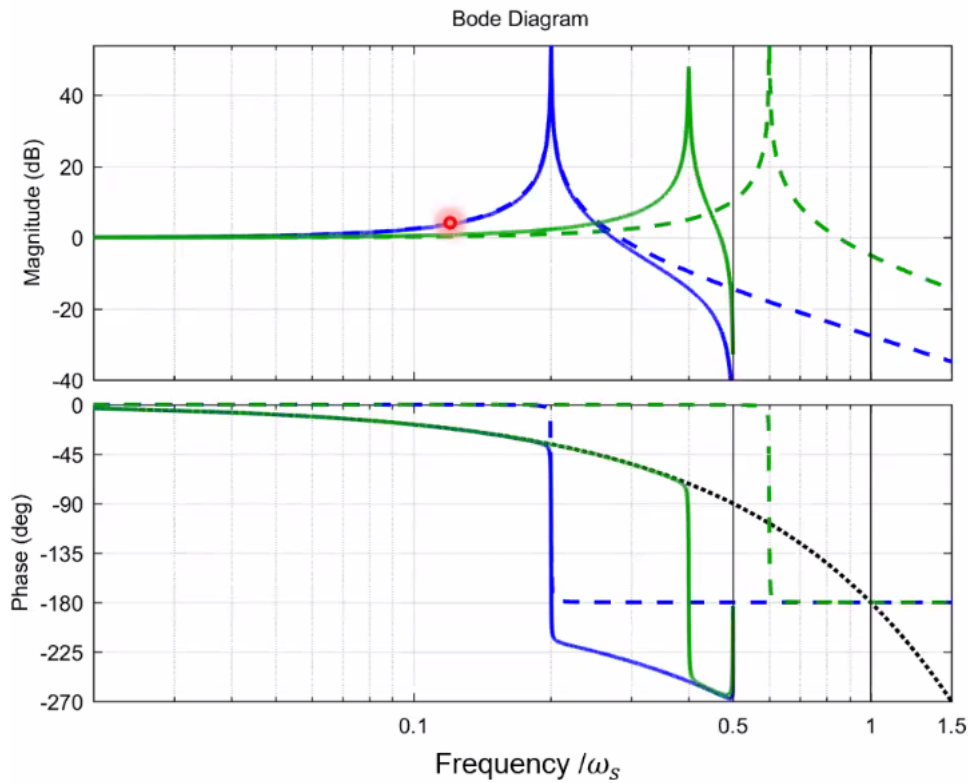


Figure 48: Aliased resonance shown on the Bode Diagram

## 3.2 Nature, Modelling and Mitigation of potentially aliasing resonances

The aliased modes can for instance come from local modes in the actuators that are lightly damped and at high frequency (Figure 50)

The proposed idea to better model aliasing resonances is to include more modes in the FEM software as shown in Figure 51 and then perform an order reduction in matlab.

## 3.3 Anti aliasing filter design

### 3.3.1 Introduction

- Anti-aliasing filtering can be used to reject aliasing of resonances and to maintain the stability of the control loop
- However, its phase lag deteriorates the control loop performances:
  - phase margin decreases (Figure 52)

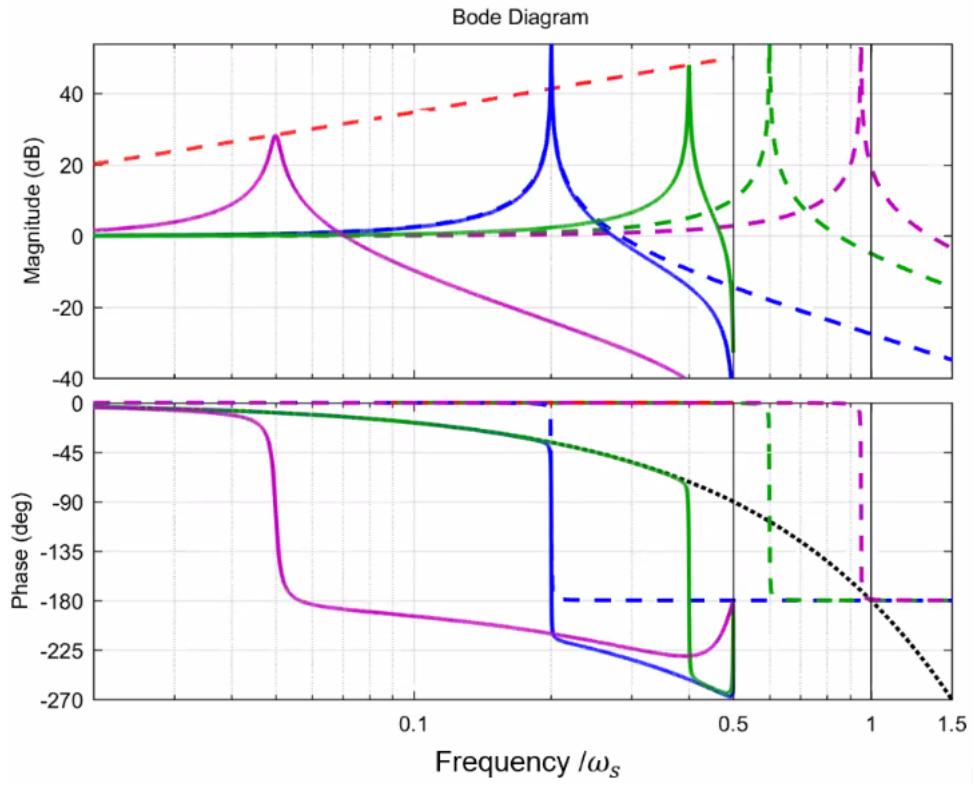


Figure 49: Higher resonance frequency

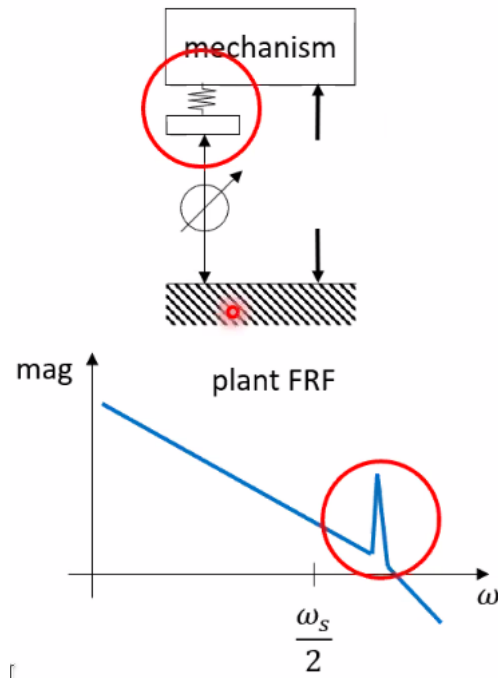


Figure 50: Local vibration mode that will be alized

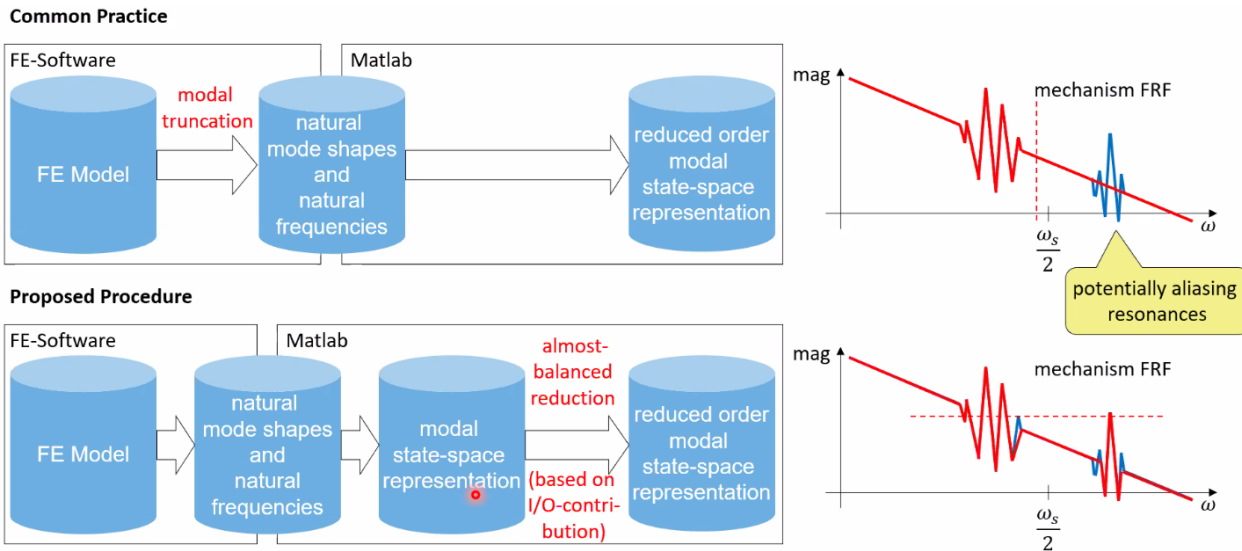


Figure 51: Common procedure and proposed procedure to include aliased resonances

– sensitivity peak increases (Figure 53)

- Thus, the anti-aliasing filter should be targeted at sufficient rejection at least possible phase lag

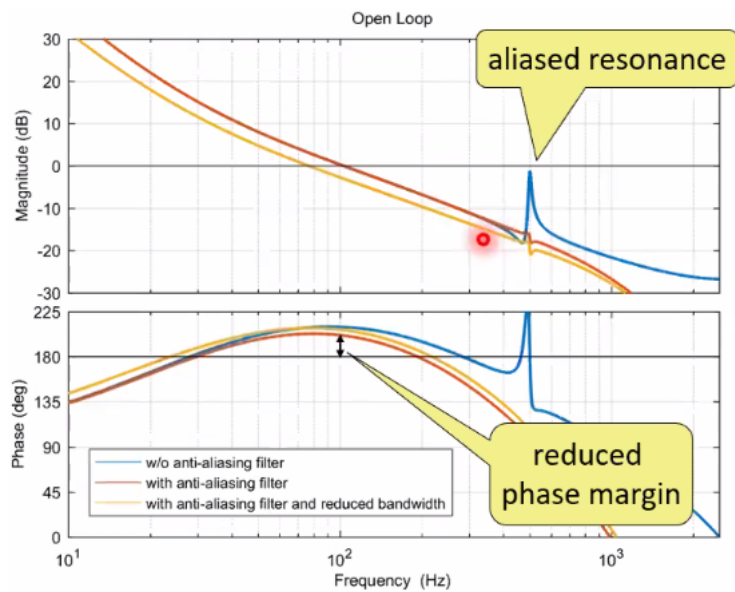


Figure 52: Example of the effect of aliased resonance on the open-loop

### 3.3.2 Concept of equivalent delay

Concept:

- At frequencies well below its poles and zeros, a continuous time filter  $F(j\omega)$  shows almost linear phase:

$$\arg(F(j\omega)) \approx -T_e\omega \quad (10)$$

on at least possible

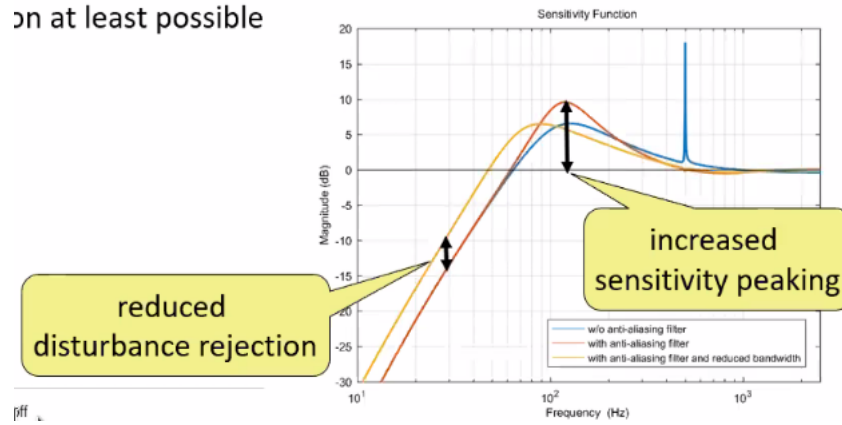


Figure 53: Example of the effect of aliased resonance on sensitivity function

- Thus, the phase lag of the filter can be fairly correctly represented by a time delay (below the pole frequency). The equivalent delay is:

$$T_e = \sum_{i=1}^{N_p} \frac{\xi_{pi}}{\omega_{0pi}} - \sum_{i=1}^{N_z} \frac{\xi_{zi}}{\omega_{0zi}} \quad (11)$$

- where  $\omega_{0pi}$  is the natural frequency  $\xi_{pi}$  is the damping of the  $N_p$  poles of  $F(s)$ . Similarly,  $\omega_{0zi}$  is the natural frequency  $\xi_{zi}$  is the damping of the  $N_z$  zeros of  $F(s)$ .

**Examples** (Figure 54):

- First order low pass filter:

$$\xi_p = 1 \Rightarrow T_e = \frac{1}{\omega_c}$$

- Second order Butterworth low pass filter:

$$\xi_p = \frac{1}{\sqrt{2}} \Rightarrow T_e = \sqrt{2} \frac{1}{\omega_c}$$

- First order lead:

$$\xi_z = 1 \Rightarrow T_e = -\frac{1}{\omega_c}$$

### 3.3.3 Budgeting of phase lag

The budgeting of the phase lag is done by expressing the phase lag of each element by a time delay (Figure 55)

The equivalent delay of each element are listed in Figure 56.

### 3.3.4 Selecting the filter order

The filter order can be chosen depending on the frequency of the resonance. Some example of Butterworth filters are shown in Figure 57 and summarized in Figure 58.

### 3.3.5 Reducing the phase lag

The equivalent delay of a low pass (here second order) depends on its damping, since:

$$T_e = -2 \frac{\xi_{zi}}{\omega_{0zi}}$$

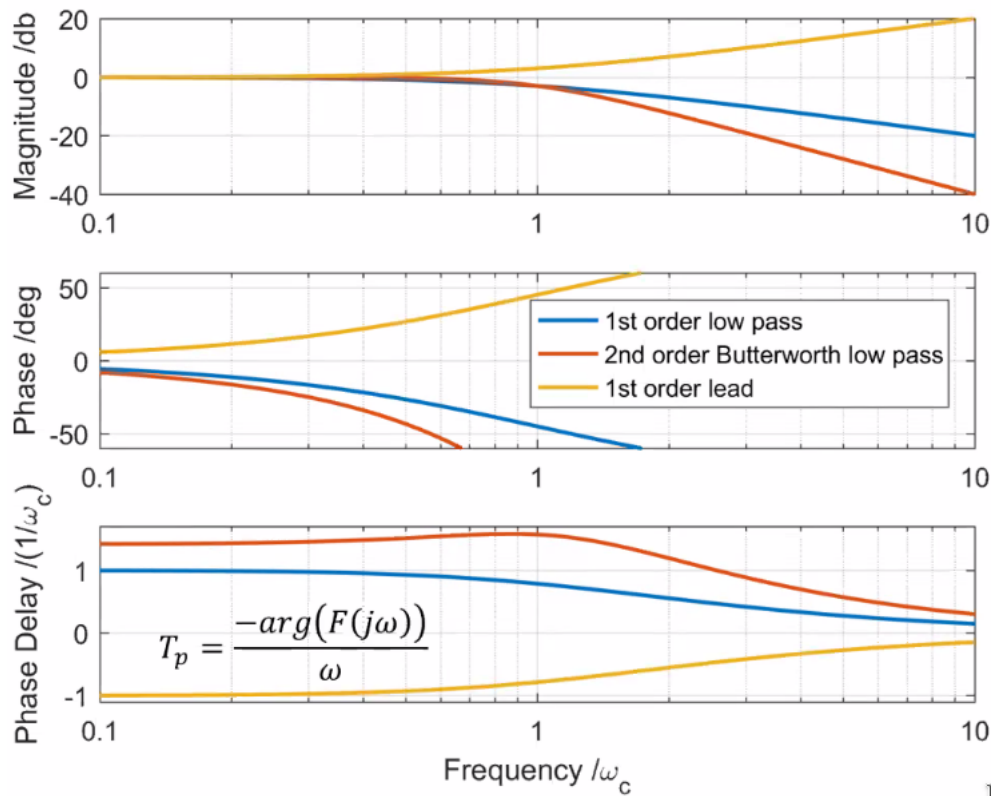


Figure 54: Magnitude, Phase and Phase delay of 3 filters

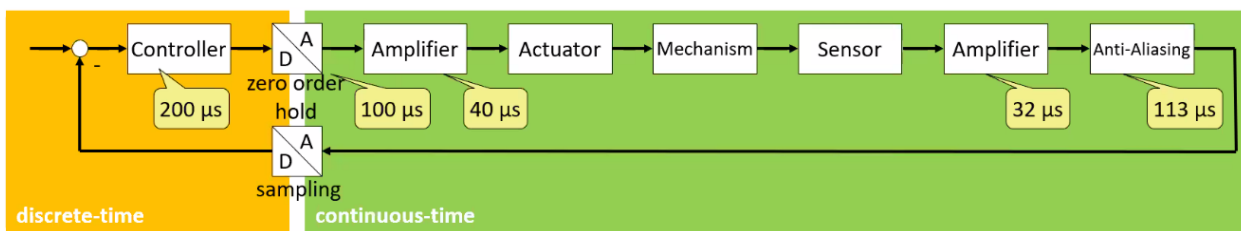


Figure 55: Typical control loop with several phase lag / time delays

	Approximation	Equivalent delay
<b>Computation time</b>	One sample step $T_s$	200 $\mu s$
<b>ZOH</b>	$T_s/2$	100 $\mu s$
<b>Actuator's current control loop</b>	Complementary sensitivity function	40 $\mu s$
<b>Sensor filter</b>	1 <sup>st</sup> order low pass at 5 kHz	32 $\mu s$
<b>Anti-aliasing filter</b>	2 <sup>nd</sup> order Butterworth at 2kHz	113 $\mu s$
<b>Total</b>		<b>485 <math>\mu s</math></b>

Figure 56: Equivalent delay for all the elements of the control loop

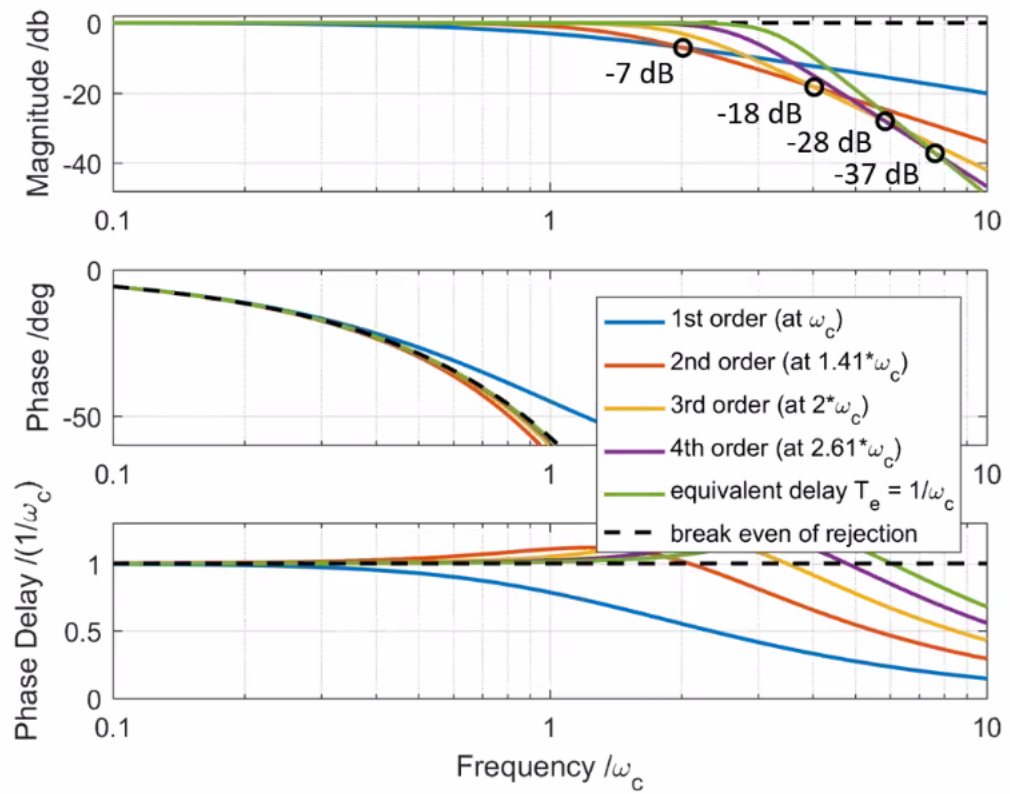


Figure 57: Example of few Butterworth filters

<b>Order</b>	1	2	3	4	5
<b>Cut-off frequency factor</b>	1	1.41	2	2.61	3.24
<b>Rejection break-even</b>	-	-7 dB	-18 dB	-28 dB	-37 dB

Figure 58: Butterworth filters



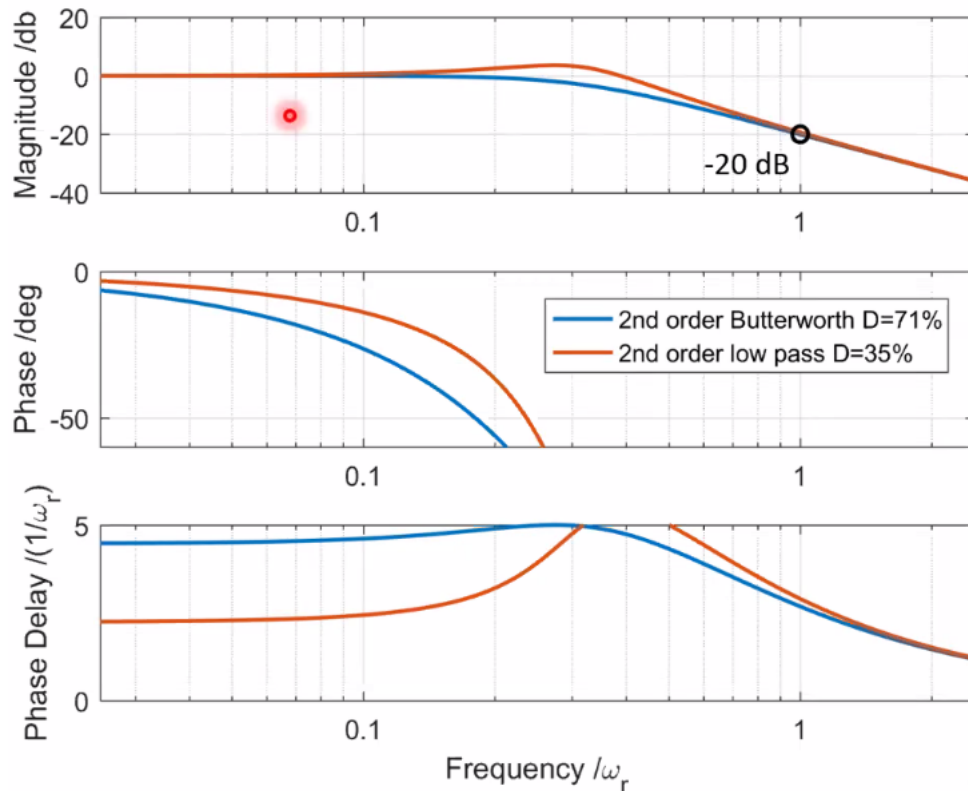


Figure 59: Change of the phase delay with the damping of the filter

### 3.4 Conclusion

The phenomenon of aliasing of resonances:

- Aliasing of resonances is an issue in discrete-time controlled mechatronic systems and **can limit the performance** and even **render the closed loop system unstable**
- Resonances above the Nyquist Frequency appear **aliased** at mirrored frequency for the discrete-time controller
- Aliased resonances show **increased damping** compared to the original resonances
- To find out if a resonance is an aliased one or not, change the sampling frequency and see if the frequency of the resonance is changing or not

Nature, modelling and mitigation of potentially aliasing resonances:

- The origin are typically local resonances of the sensor and actuator components
- Careful modelling and selecting dominant modes above the Nyquist frequency is commended

Anti-aliasing filter design:

- Anti-Aliasing filter design is the **trade-off between rejection and phase-lag**
- The concept of **equivalent delay** allows to budget and design the phase lag
- The order selection of anti aliasing-filter based on the required rejection is shown
- Several approaches to reduce overall phase lag are presented

## 4 Flexure positioning stage based on delta technology for high precision and dynamic industrial machining applications @mikael\_bianchi

### 4.1 Introduction

- **Goal:** flexure positioning stage to do high precision and high dynamic/acceleration positioning. The control architecture should be as simple as possible.
- **Application:** micromachining for fabrication of 3d structures
- **Possible field:** watch industry, electronics, optics, ...
- **Possible technologies:** laser, milling, electro discharge machine
- **Objectives:** improve the productivity reaching high accelerations at high precision

### 4.2 Design

#### 4.2.1 Description of the Delta robot

**Technical choice:** flexure based delta robot (Figure 60).

- **Advantages:** high mechanical precision without backlash
- **Disadvantage:** the motion is coupled, some transformations are required from motor coordinates to machine coordinates (Figure 61)

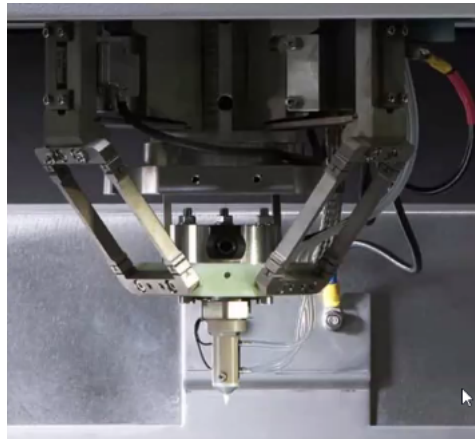


Figure 60: Picture of the Delta Robot

#### 4.2.2 Modelling and validation of the delta robot

Lagrange equations are used to model the dynamics of the delta robot. The motor positions are used as the general coordinate system.

The system is then linearized around the working point (Figure 62).

Then the parameters are identified from experiment (Figure 63).

The measurement of the coupling is more complicated as shown in Figure 64.

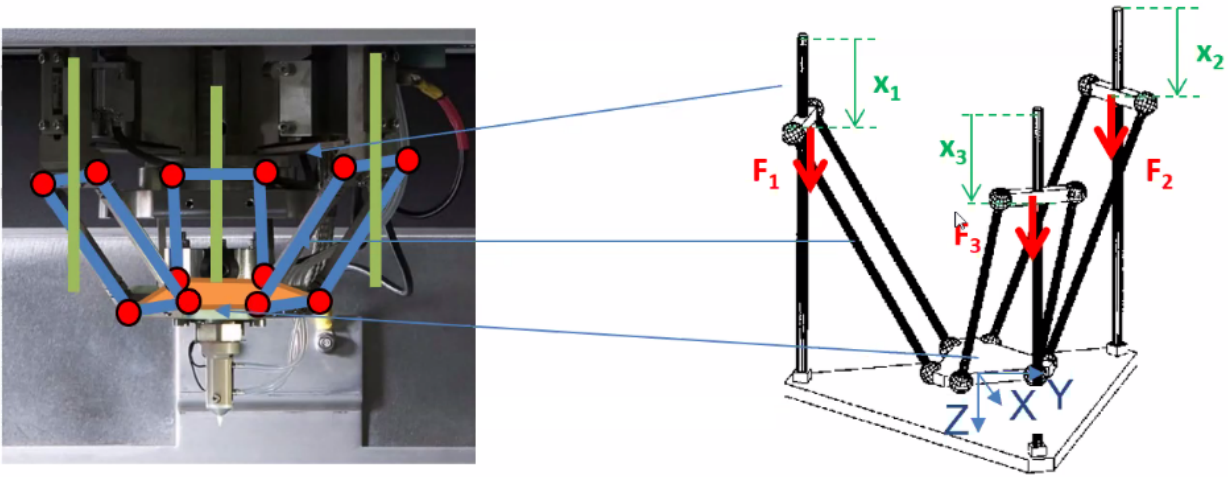


Figure 61:  $x_1, x_2, x_3$  are the motor positions.  $f_1, f_2, f_3$  are the force motors.  $x, y, z$  are the position of the final point in cartesian coordinates

$$\begin{bmatrix} 1 & 0 & 0 & 0 & 0 & 0 \\ 0 & 1 & 0 & 0 & 0 & 0 \\ 0 & 0 & 1 & 0 & 0 & 0 \\ 0 & 0 & 0 & M & M_{cr} & M_{cr} \\ 0 & 0 & 0 & M_{cr} & M & M_{cr} \\ 0 & 0 & 0 & M_{cr} & M_{cr} & M \end{bmatrix} \begin{bmatrix} \dot{x}_1(t) \\ \dot{x}_2(t) \\ \dot{x}_3(t) \\ \dot{v}_1(t) \\ \dot{v}_2(t) \\ \dot{v}_3(t) \end{bmatrix} = \begin{bmatrix} 0 & 0 & 0 & 1 & 0 & 0 \\ 0 & 0 & 0 & 0 & 1 & 0 \\ 0 & 0 & 0 & 0 & 0 & 1 \\ k_p & k_{p,cr} & k_{p,cr} & k_v & 0 & 0 \\ k_{p,cr} & k_p & k_{p,cr} & 0 & k_v & 0 \\ k_{p,cr} & k_{p,cr} & k_p & 0 & 0 & k_v \end{bmatrix} \begin{bmatrix} x_1(t) \\ x_2(t) \\ x_3(t) \\ v_1(t) \\ v_2(t) \\ v_3(t) \end{bmatrix} + \begin{bmatrix} 0 & 0 & 0 \\ 0 & 0 & 0 \\ 0 & 0 & 0 \\ 0 & 0 & 0 \\ 0 & kT & 0 \\ 0 & 0 & kT \end{bmatrix} \begin{bmatrix} I_1(t) \\ I_2(t) \\ I_3(t) \end{bmatrix}$$

Coupled mass matrix [Kg]      Coupled elasticity matrix [N/m]      Friction [N/(m/s)]      Force constant [N/A]

Prediction error / nonparametric      Static force measure      Prediction error / nonparametric      Datasheet/static force measure

Figure 62: Linearized equations of the Delta Robot

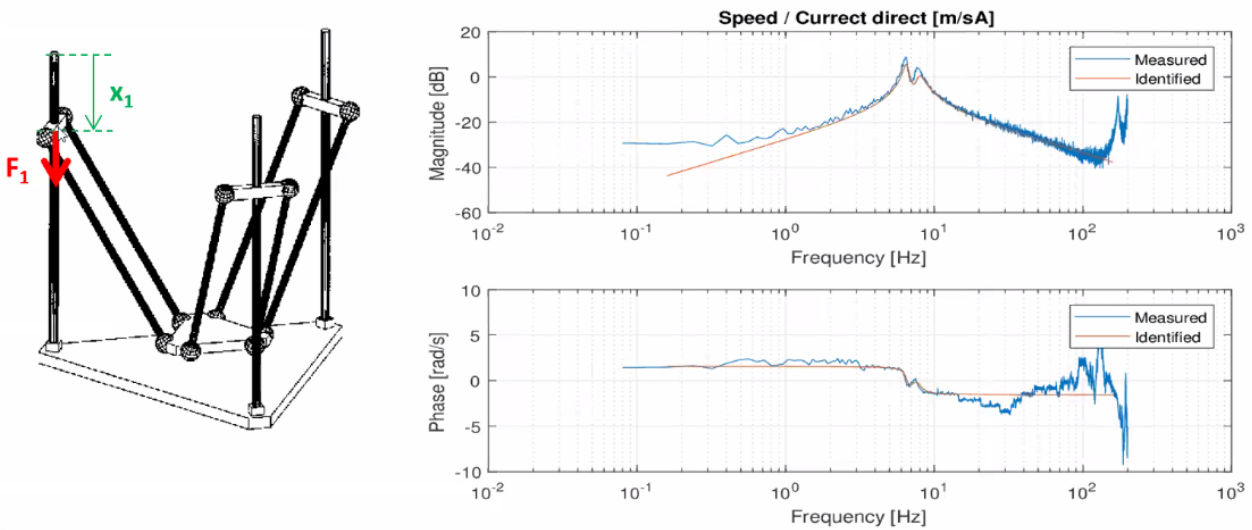


Figure 63: Identification for the transfer function from  $F_1$  to  $x_1$

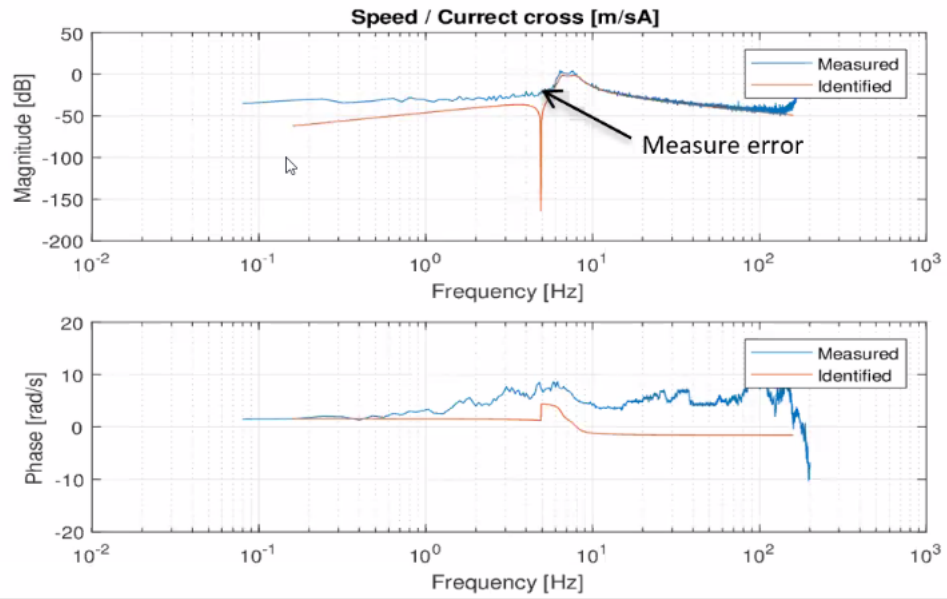


Figure 64: Problem of identifying the coupling between F1 and x2 at low frequency

#### 4.2.3 Control design for high trajectory tracking

Control requirements:

- Precise position control of the coupled system (+/-10nm steps)
- Minimal trajectory error at high frequency (+/- 100nm at +/- 1g acceleration)
- Higher resonances attenuation
- Whole motion system is considered as a standard cartesian XYZ axes for the user (do the inverse/forward kinematics inside the control architecture)

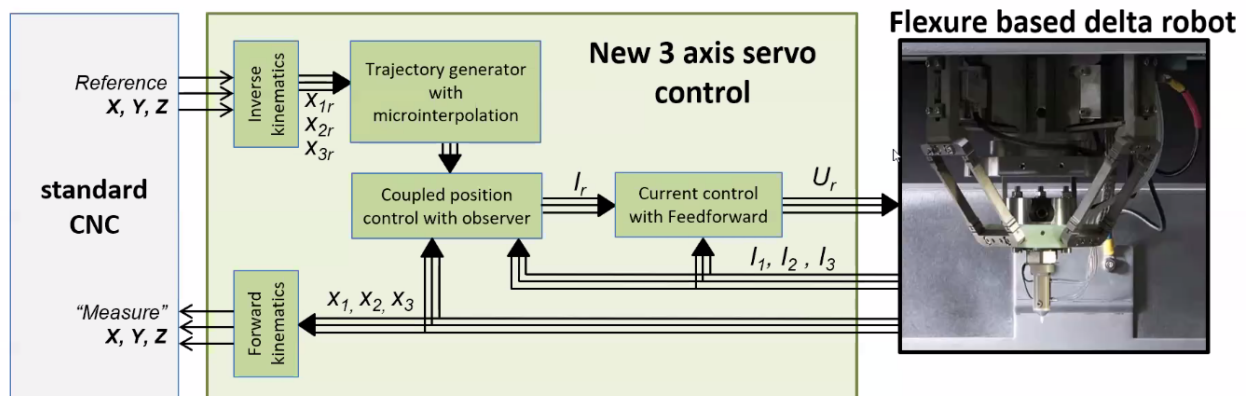


Figure 65: Control concept used for the Delta robot

#### 4.2.4 Electronic board

A 3 axis servo control board as been developed (Figure 66) which includes:

- identification algorithm of the coupled system integrated in the board
- interpolator for sensors

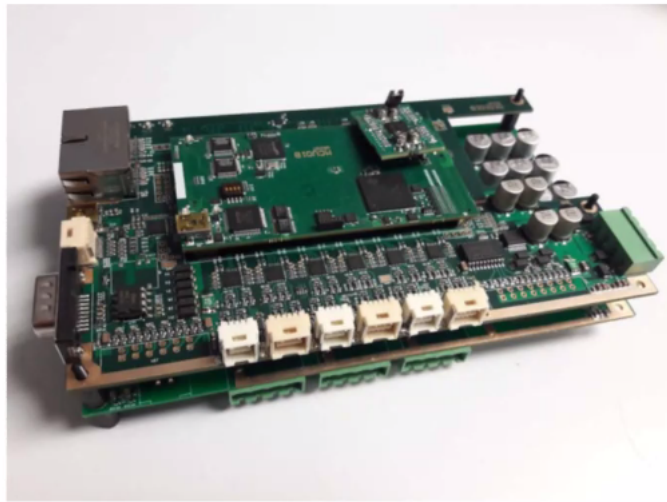


Figure 66: Servo control board

]

## 4.3 Results

### 4.3.1 Current control

Step response of the current control loop is shown in Figure 67.

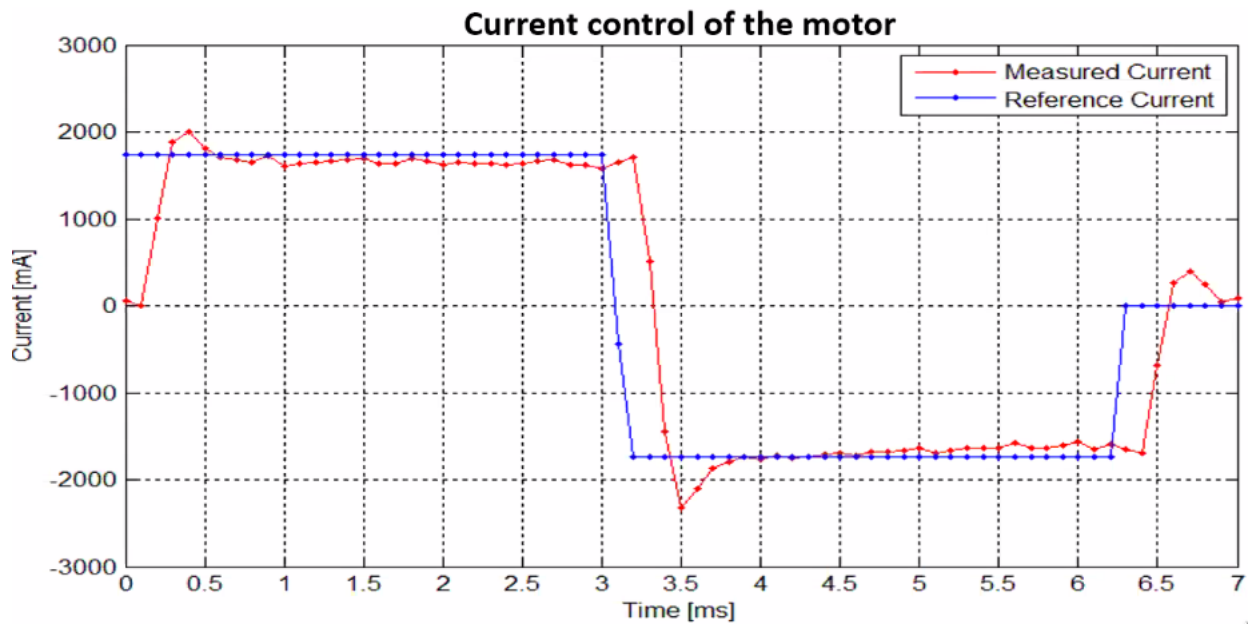


Figure 67: Step response for the current control loop

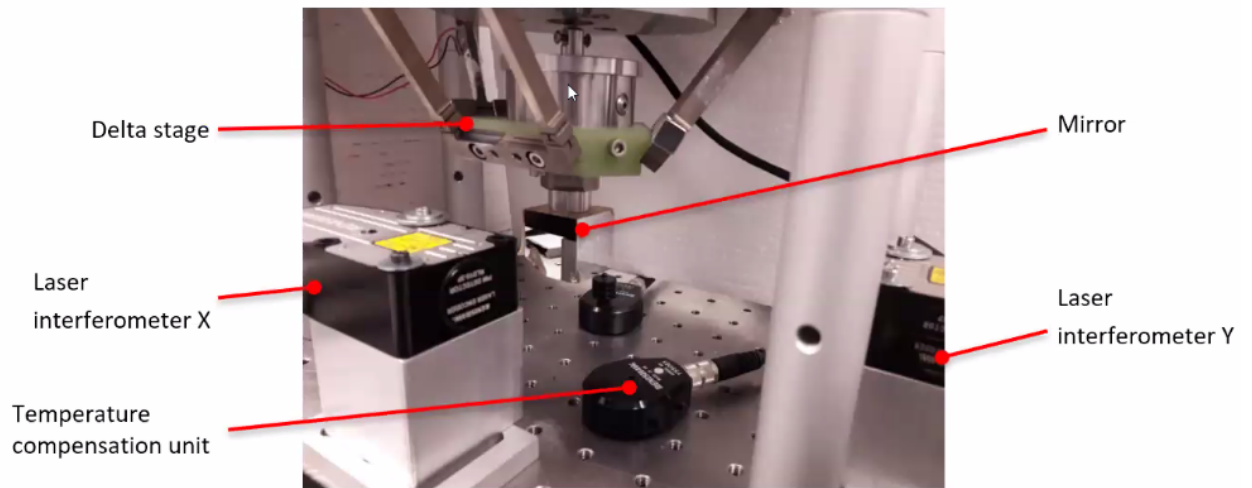


Figure 68: Experimental setup to verify the performances of the system

#### 4.3.2 Trajectory tracking: results with laser interferometer and encoder

XY renishaw interferometers used to verify the performance of the system (Figure 68).

Some results are shown in Figures 69, 70 and 71.

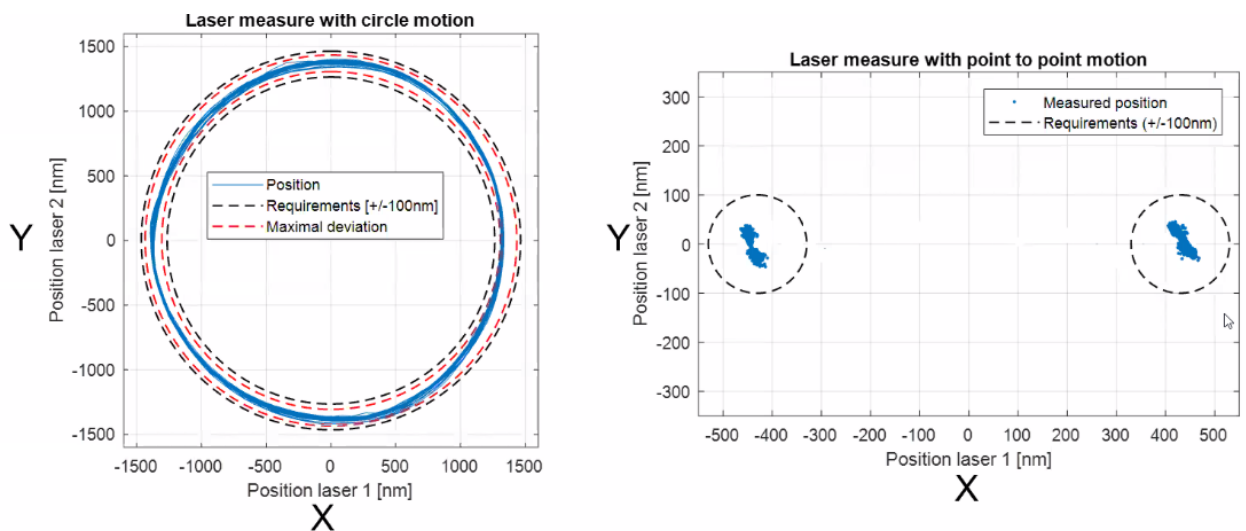


Figure 69: Circuit motion results and point to point motion results

#### 4.4 Conclusion

As a conclusion, here are the identified conditions for precise and high dynamic positioning:

- Mechanics **without backlash** and **resonances in higher frequency**
- **Feedforward** with correct parameters
- **High bandwidth** position control and precise encoder
- Low noise current sensors and high bandwidth current control

Resonances at mid frequencies are an issue for further improvements.

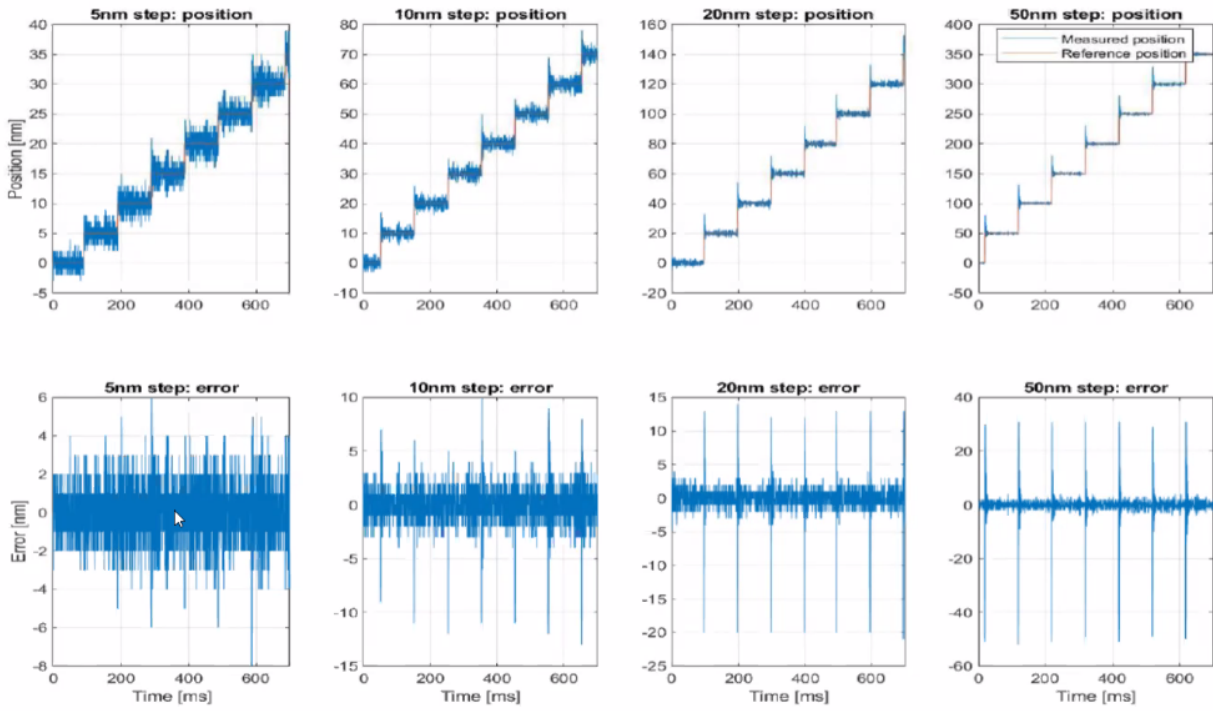


Figure 70: Step response of the system

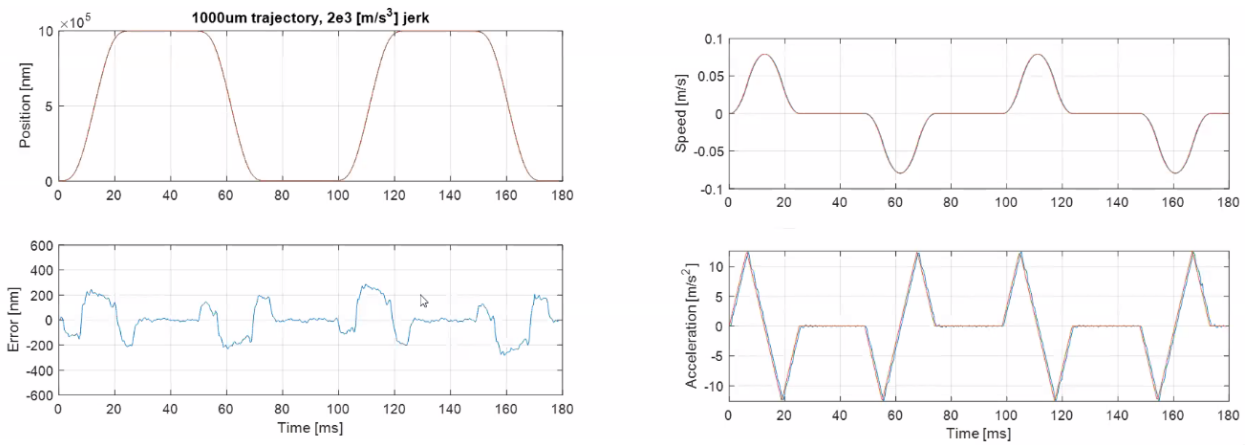


Figure 71: Measured dynamical errors

# 5 Multivariable performance analysis of position-controlled payloads with flexible eigenmodes

@luca\_mettenleiter

## 5.1 Motivation

Flexible eigenmodes are present in every system component and leads to:

- controller bandwidth limitation (Figure 72)
- additional cross-coupling in the system behavior (Figure 73)

=> can lead to stability problems

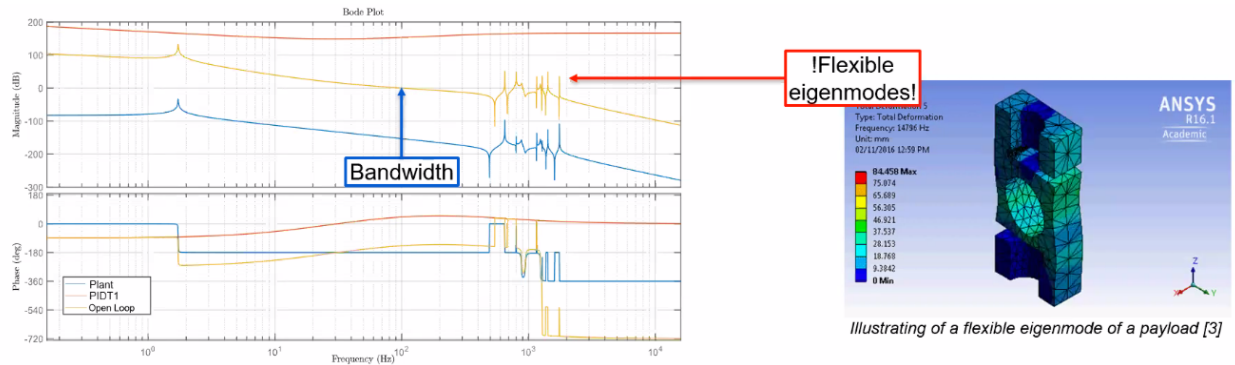


Figure 72: Limitation of the control bandwidth due to flexible eigenmodes

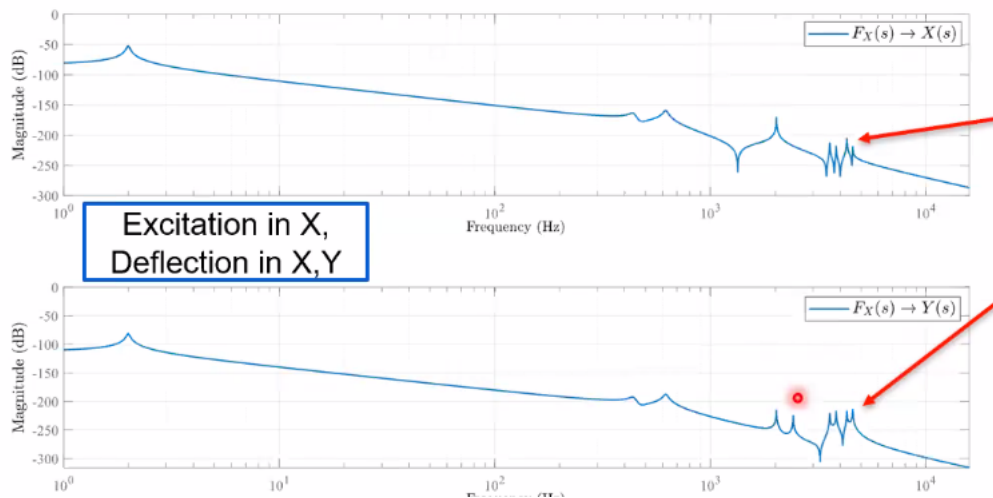


Figure 73: Coupling due to flexible eigenmodes

In order to estimate the performances of a system, the sensitivity function can be used (Figure 74).

## 5.2 Performance analysis with different sensitivity functions

There are different way to analyse the sensitivity function base on different plants (Figure 75):

1. the **full system** (complicated):

$$L_{full} = \begin{bmatrix} L_{11} & L_{12} \\ L_{21} & L_{22} \end{bmatrix}$$



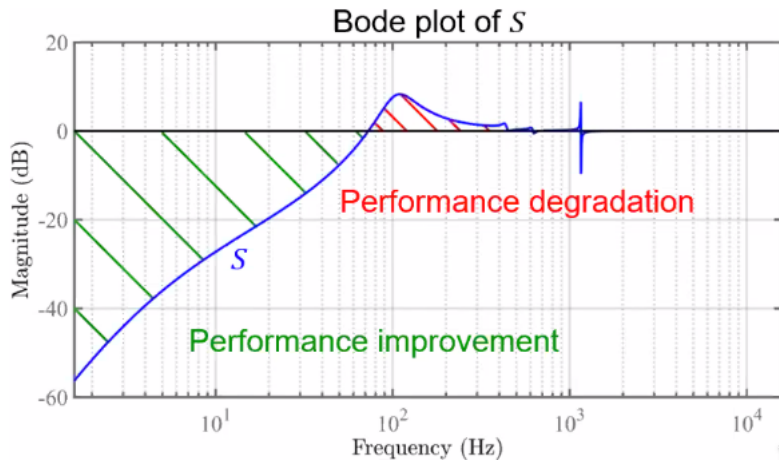


Figure 74: Bode plot of a typical Sensitivity function

2. the **diagonal system** (ignoring interaction)

$$L_{diag} = \begin{bmatrix} L_{11} & 0 \\ 0 & L_{22} \end{bmatrix}$$

3. the **loop interaction system** (the one proposed here)

$$L^{LI} = \begin{bmatrix} L_1^{LI} & 0 \\ 0 & L_2^{LI} \end{bmatrix}$$

The loop interaction methods created a SISO system that also represents the coupling in the system. One loop is closed at a time, and the coupling effects are taken into account.

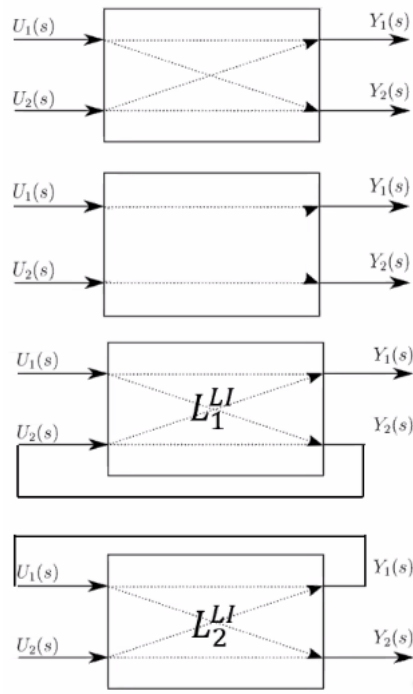


Figure 75: Visual representation of the three systems

### 5.3 Example system

In order to compare the use of the three systems to estimate the performances of a MIMO system, the system shown in Figure 76 is used. The 4 top masses are used to represent a payload that will add coupling in the system due to its resonances.

A diagonal PID controller is used.

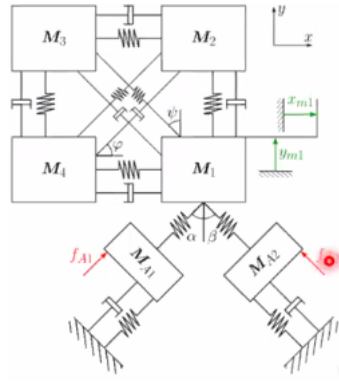


Figure 76: Schematic representation of the example system

The bode plot of the MIMO system is shown in Figure 77 where we can see the resonances in the off-diagonal elements.

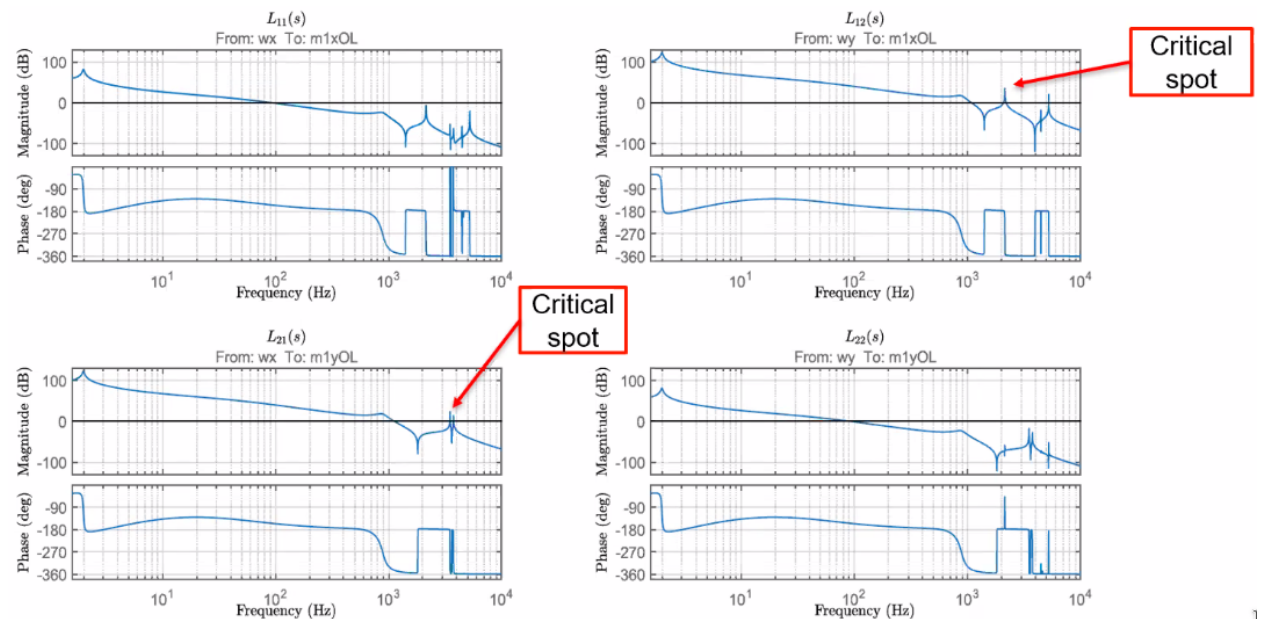


Figure 77: Bode plot of the full MIMO system

In Figure 78 is shown that the sensitivity function computed from the SISO system is not correct. Whereas for the “interaction method” system, it is correct and almost match the full system sensibility. However, as expected, the off-diagonal sensibilities are not modelled.

### 5.4 Conclusion

The conclusion are the following and summarized in Figure 79:

- Choice of suitable analysis method is key concept in mechatronics engineering

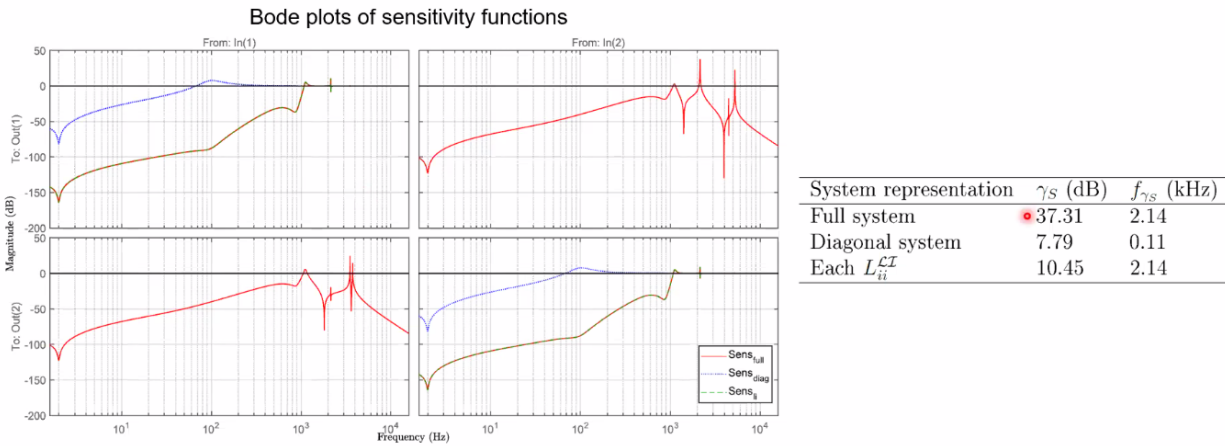


Figure 78: Bode plots of sensitivity functions

- Various methods for analysis of multivariable systems available:
  - Full system always delivers reliable information, but much analysis effort
  - Loop interaction method delivers reliable information, only if the system is weakly or symmetrically coupled
  - Diagonal system delivers unreliable information, as it does not take multivariable character into account

Method	Information about amplitude	Information about frequency	Number of functions / plots for $m \times m$ system
Diagonal System	✘	✘	$m$
Loop Interaction System	👍/✘	👍/✘	$m$
Full System	👍	👍	$m^2$

Figure 79: Comparison of the three methods to deal with a MIMO system

## 6 High-precision motion system design by topology optimization considering additive manufacturing @arnoud\_delissen

### 6.1 Introduction

The goal of this project is to perform a topology optimization of a 6dof magnetic levitated stage suitable for vacuum.

For the current system (Figure 80), the bandwidth is limited by the short-stroke dynamics (eigenfrequencies).

The goal here is to make the eigen-frequency higher as this will allow more bandwidth.

### 6.2 Case

More precisely, the goal is to automatically maximize the three eigen-frequencies of the system shown in Figure 81.

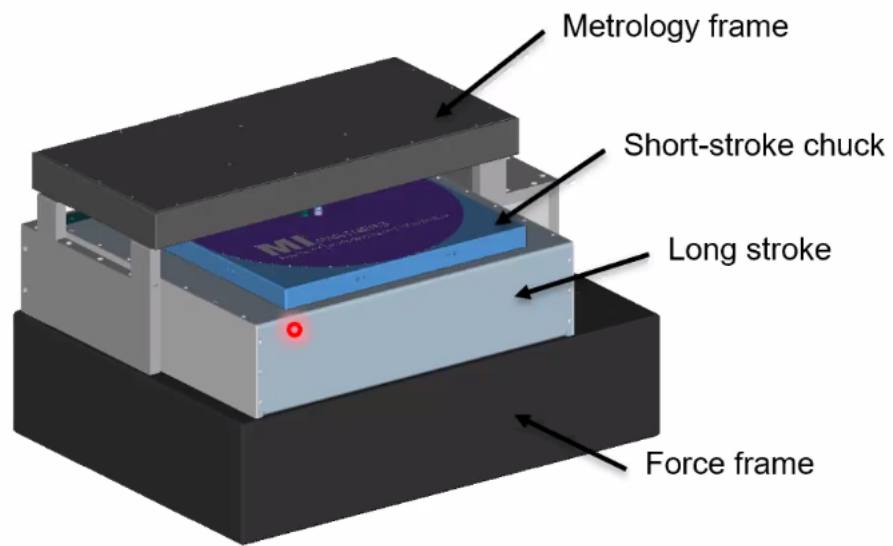


Figure 80: Schematic of the 6dof levitating stage

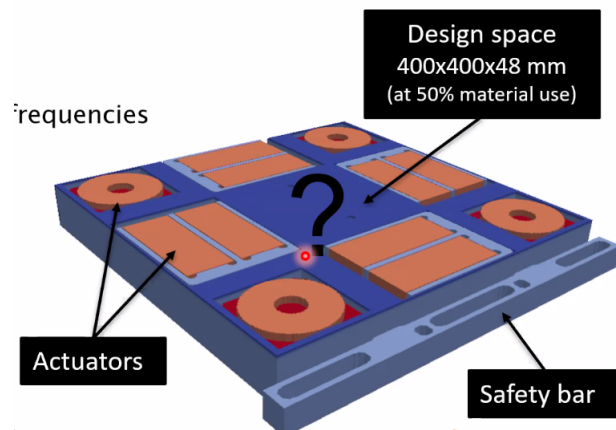


Figure 81: System to be optimized

### 6.3 Manufacturing process

The manufacturing process must be embedded in the optimization such that the obtained design is producible. The process is shown in Figure 82.



Figure 82: Manufacturing process

### 6.4 Topology optimization

**Problem:** for a given volume, maximize the eigen-frequencies of the system.

To do so, the system is discretized into small elements (Figure 83). Then, a Finite Element Analysis is performed to compute the eigen-frequencies of the system. Finally, for each element, the “gradient is computed” and we determine if material should be added or removed.

This is done in 3D. The individual 1mm x 1mm x 1mm elements are shown in Figure 83. The number of elements is 1 million ( $\Rightarrow$  15 minutes per iteration to compute the 3 eigen-frequencies).

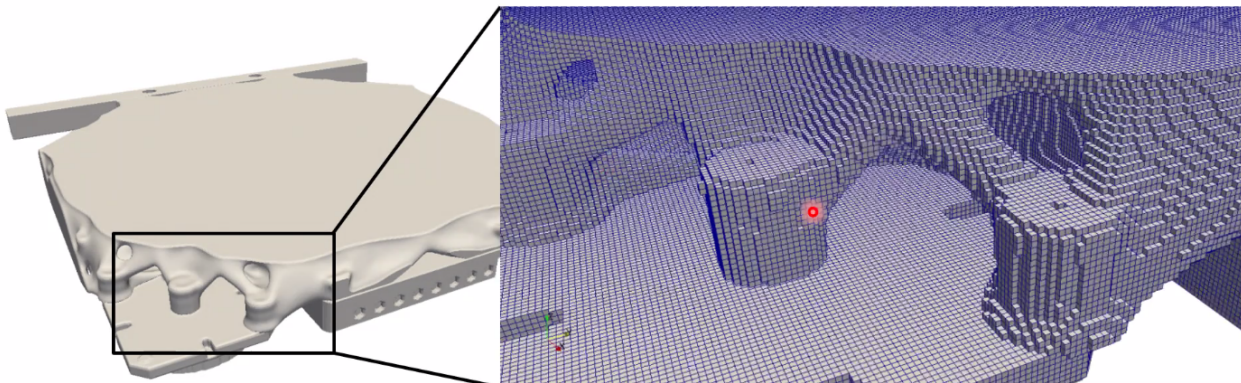


Figure 83: Results of the topology optimization and zoom to see individual elements

### 6.5 Performance Comparison

The obtained mass and eigen-frequencies of the optimized system and the solid equivalents are compared in Figure 84.

Identification on the realized system shown that the obtained eigen-frequencies are very closed to the estimated ones (Figure 85).

### 6.6 Conclusion

- Increase in performance ( $\sim 2x$ ) compared to solid designs
- A design is obtained in  $\sim 1$  day
- Practical constraints are incorporated in the optimization

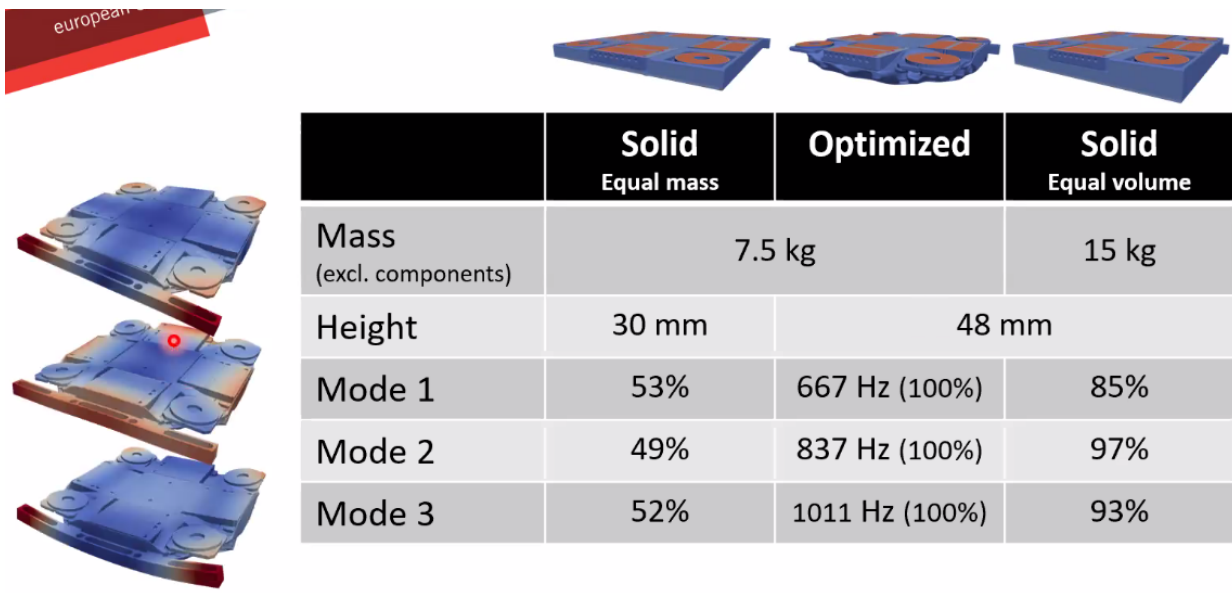


Figure 84: Comparison of the obtained performances

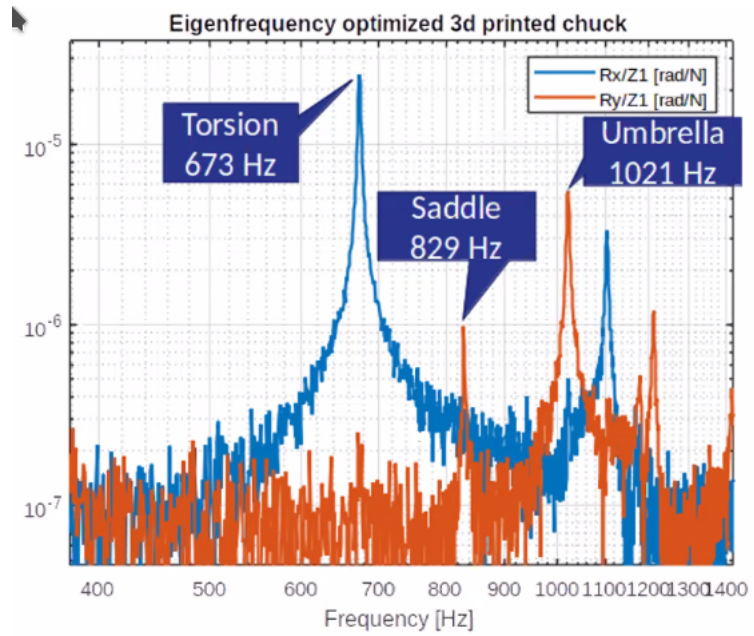


Figure 85: Results very close to simulation ( $\sim 1\%$  for the eigen frequencies)

- The method is validated in practice by a demonstrator

## 7 A multivariable experiment design framework for accurate FRF identification of complex systems @nic\_dirkx

### 7.1 Introduction

**Goal:** Need for higher quality FRF models that are used to:

- Controller design
- Observer design
- System diagnostics
- Parametric modelling

High quality FRFs requires careful design of excitation  $w$ .

Typical experimental identification of the FRFs is shown in Figure 86.

The design trade-off is:

- Maximize input gain to minimize FRF uncertainty
- Bounded signal  $u$  and  $y$  to remain within operating limited (actuator/amplifier power limitations and limited move ranges)

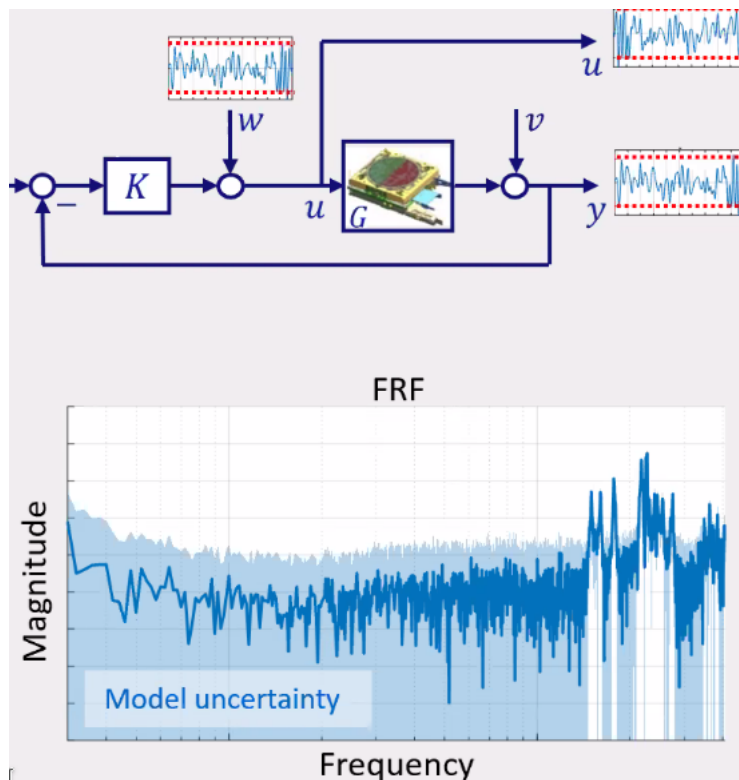


Figure 86: schematic of the identification of the FRF

For SISO systems:

- Only the frequency size of the excitation signal should be optimized

For MIMO systems:

- the gains and **directions** should be frequency wise optimized

**Objective:**

- establish optimal experiment design framework that optimize the excitation signal to obtain MIMO FRFs with low uncertainty

## 7.2 Role of directions and constrains in multivariable excitation design

The classical way to estimate MIMO FRFs is the following:

- First start with one direction and increase the gain until constrains is attained (Figure 87)
- Do the same with the second input

This lead to non-optimal FRFs estimation.

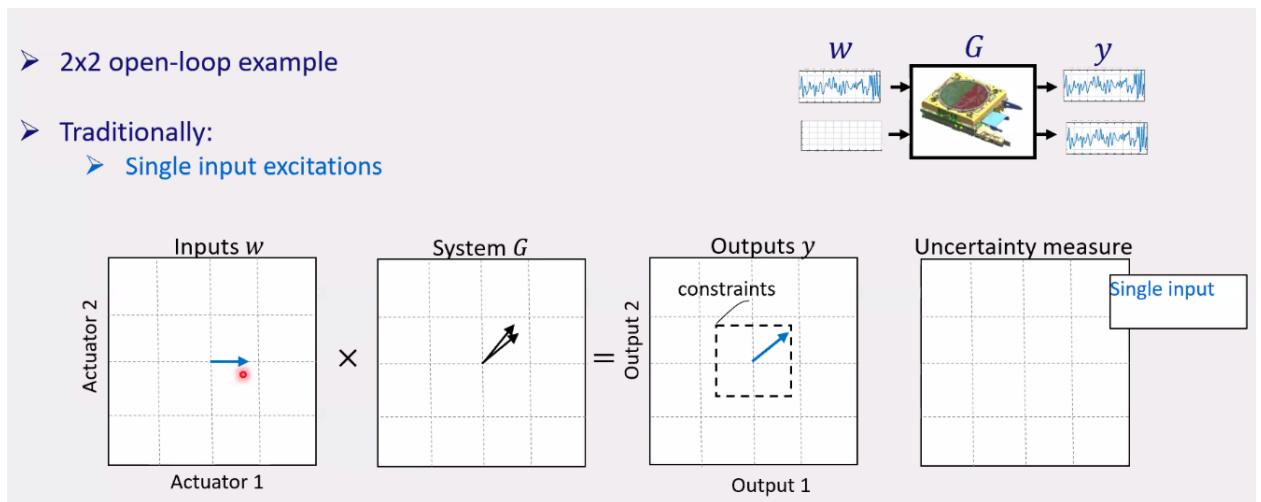


Figure 87: Example of a SISO approach to identify MIMO FRFs

When having a MIMO approach and choosing both the direction and gain of the excitation inputs, we can obtain much better FRFs uncertainty while still fulfilling the constraints (Figure 88).

## 7.3 Solving the optimization problem

The optimization problem is to minimize the model uncertainty by choosing the design variables which are the magnitude and direction of the inputs  $w$ .

The optimization is a two step process as shown in Figure 89:

1. first identification without optimization that allows to have data to run the optimization process
2. second identification with optimized input direction and gain

The problem with this optimization problem is that it is not convex in general and has a log of design variables. There is no general method to solve this problem, a dedicated algorithm is required.

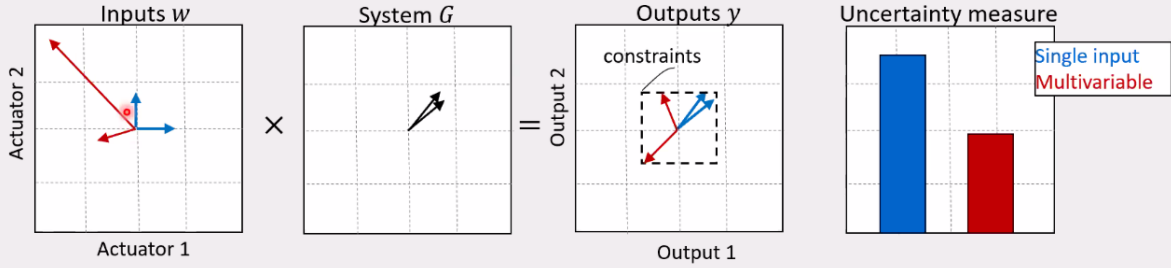
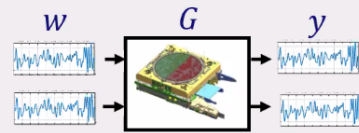
In this work, two algorithms are proposed and not further detailed here.



➤ 2x2 open-loop example

➤ Traditionally:

- Single input excitations
- Directions are fixed regardless of  $G$ , non-optimal



➤ Optimal excitations are **multivariable** and have gains and directions tailored to system!

Figure 88: Example of the MIMO approach that gives much better FRFs

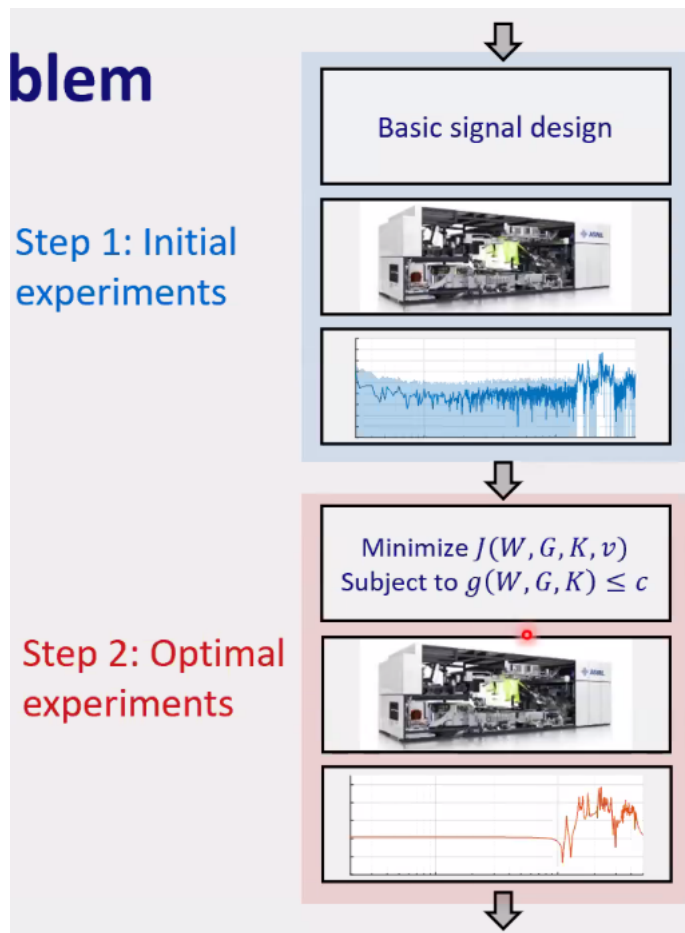


Figure 89: Two step optimization process

## 7.4 Experimental validation

Experimental identification of a 7x8 MIMO plant was performed in for different cases:

1. non optimized SISO approach (grey)
2. optimized SISO approach (blue)
3. optimized MIMO approach using SSDR (first algorithm proposed) (green)
4. optimized MIMO approach using RR (second algorithm proposed) (red)

The obtained FRFs are shown in Figure 90.

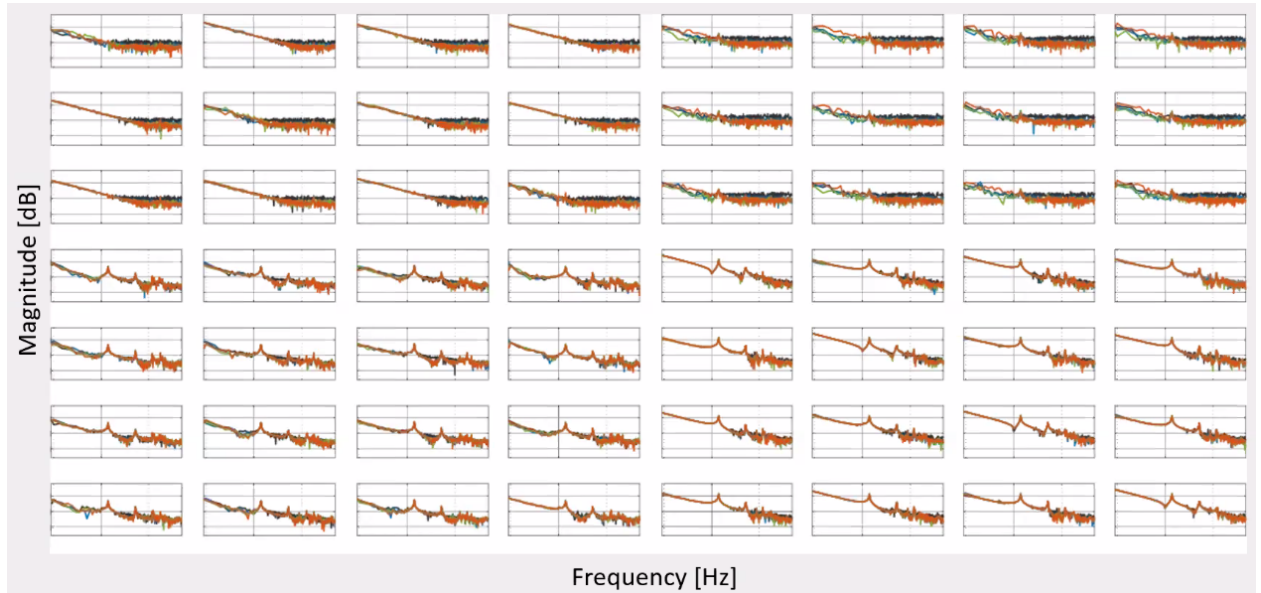


Figure 90: Obtained MIMO FRFs

A comparison of one of the obtained FRFs is shown in Figure 91. It is quite clear that the MIMO approach can give much lower FRF uncertainty. The RR proposed algorithm is giving the best results

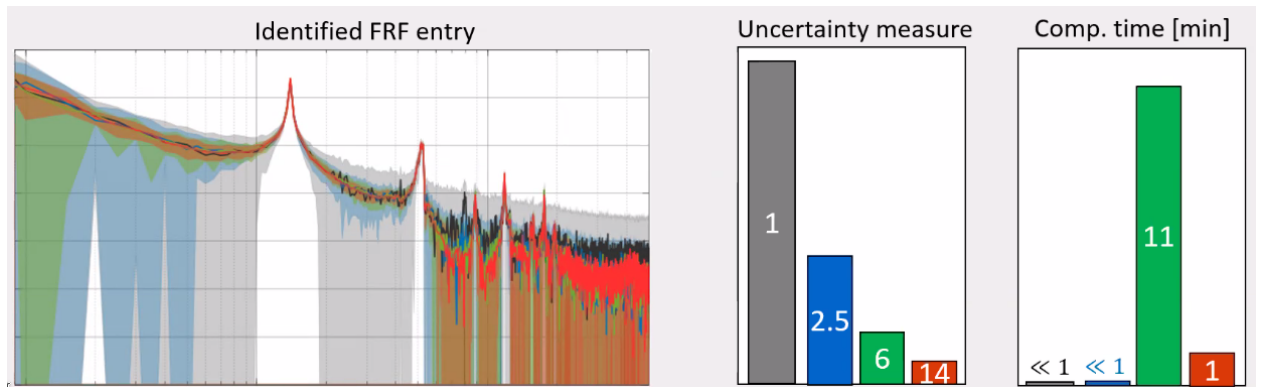


Figure 91: Example of one of the obtained FRF

## 7.5 Conclusion

- The uncertainty of the obtained FRF are obtained by doing several experimental identification with a deterministic input signal. The FRF are computed multiple times, and the spread of the results at each frequency represents this uncertainty.

- Exploiting directionality in excitation design enables significant FRF quality improvement
- Multivariable design involves hard non-convex optimization problem
- Computationally tractable design framework for large scale MIMO systems established
- Near global optimal quality achieved on wafer stage setup using RR algorithm

## 8 Keynote: High precision mechatronic approaches for advanced nanopositioning and nanomeasuring technologies @eberhard\_manske

### 8.1 Coordinate Measurement Machines (CMM)

Examples of Nano Coordinate Measuring Machines are shown in Figure 92.



Figure 92: Example of Coordinate Measuring Machines

### 8.2 Difference between CMM and nano-CMM

With classical CMM, the Abbe-principle is not fulfilled in the x and y directions (Figure 93).

The Abbe error can be determined with:

$$\Delta l_{x,y,z} = l_{x,y,z} \sin \Delta \phi_{x,y,z} \quad (12)$$

Even with the best spindle:  $l_{x,y} = 100mm$  and  $\Delta \phi = 2arcsec$ , we obtain an error of:

$$\Delta l = 0.1\mu m \quad (13)$$

which is not compatible with nano-meter precisions.

Then, the classical CMM will not work for nano precision

### 8.3 How to do nano-CMM

High precision mechatronic approaches are required for advanced nano-positioning and nano-measuring technologies:

- High precision measurement concept

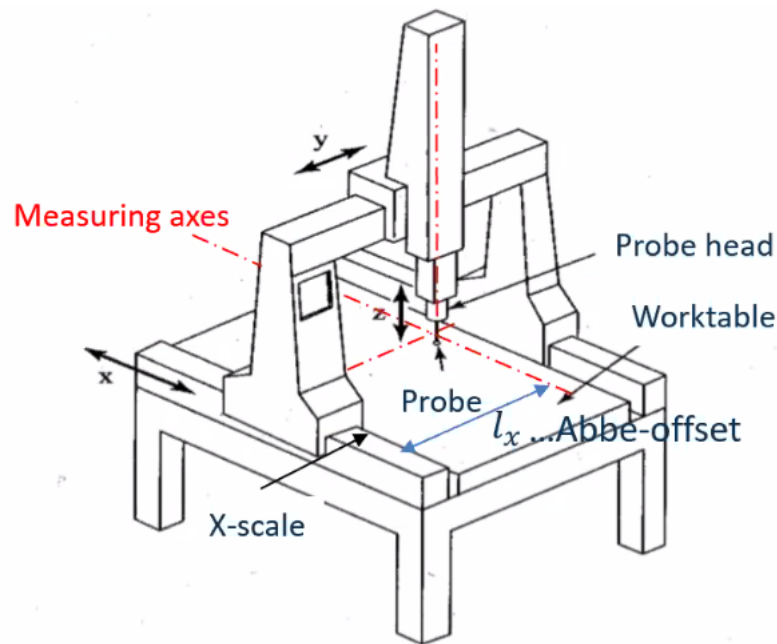


Figure 93: Schematic of a CMM

- High precision measurement systems
- High precision nano-sensors

Combined with:

- Advanced automatic control
- Advanced measuring strategies

#### 8.4 Concept - Minimization of the Abbe Error

In order to minimize the Abbe error, the measuring “lines” should have a common point of intersection (Figure 94).

The 3D-realization of Abbe-principle is as follows:

- 3 interferometers: cartesian coordinate system
- probe located as the intersection point of the interferometers

#### 8.5 Minimization of residual Abbe error

Still some residual Abbe error can happen as shown in Figure 95 due to both a change of angle and change of position.

#### 8.6 Compare of long travel guiding systems

In order to have the Abbe error compatible with nano-meter precision, the precision of the spindle should be less and one arcsec which is not easily feasible with air bearing or precision roller bearing technologies as shown in Figure 96.

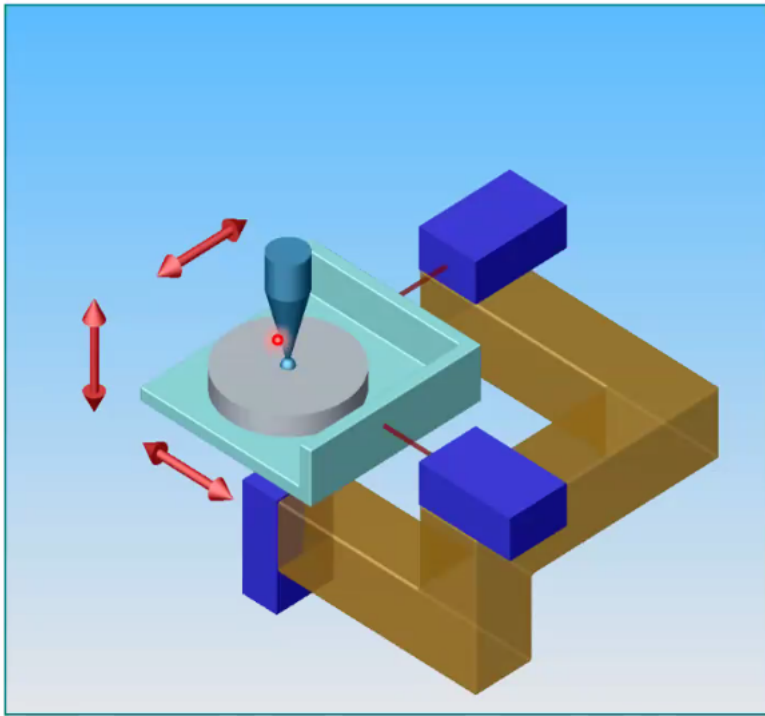
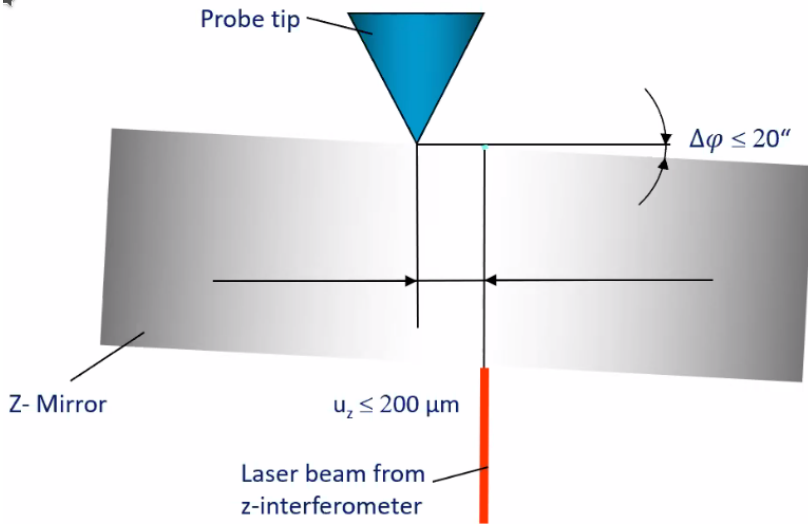


Figure 94: Error minimal measuring principle



$$\Delta l_{x,y,z} = l_{x,y,z} \cdot \sin\Delta\varphi_{x,y,z}$$

$$l_{x,y,z} = 0 \pm u_{x,y,z}$$

for  $u_z < 200 \mu\text{m}$

residual error:  $\Delta l \leq 20 \text{ nm}$



goal:  $< 1 \text{ nm}$  Abbe-error

additional requirement:

$$\Delta\varphi_{x,y,z} \rightarrow 0$$

angular deviation:  $< 1 \text{ arcsec}$ .

Figure 95: Residual Abbe error

	air bearing	precision roller bearing
moving mass	large	smaller
dynamics	limited	better
costs	expensive	moderately
angular deviation	2 arcsec.	20 arcsec.
Abbe error ( $l_{\text{off}}=200 \mu\text{m}$ )	2 nm	20 nm
Requirement: < 1 arcsec.	technically not feasible	

Figure 96: Characteristics of guidings

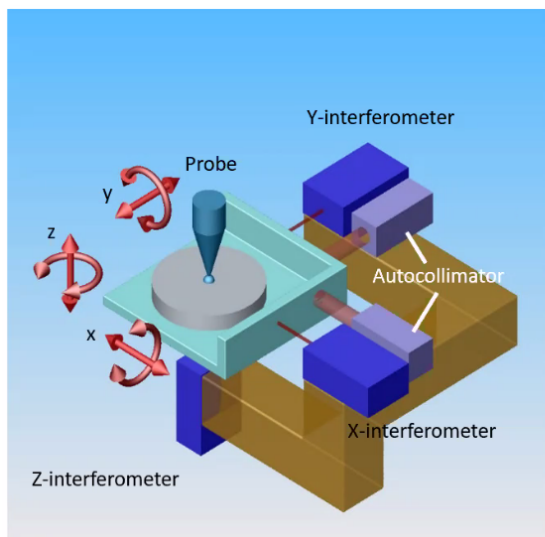
### 8.7 Extended 6 DoF Abbe comparator principle

The solution used was to measure in real time the angles of the frame using autocollimators as shown in Figure 97 and then to minimize this tilt by close loop operation with additional actuators.

The angular measurement error and control is less than 0.05 arcsec which make the residual Abbe error:

$$\Delta l < 0.05 \text{ nm} \quad (14)$$

Without an error-minimal approach, nano-meter precision cannot be achieved in large areas.



- Measurement of tilt errors by autocollimators
- Minimization of tilt by close loop operation with additional actuators

Angular measurement and control: < 0.05 arcsec.

Residual Abbe error:  $\Delta l_i < 0.05 \text{ nm}$

Without an error-minimal approach, nanometer precision cannot be achieved in large areas.

Figure 97: Use of additional autocollimator and actuators for Abbe minimization

### 8.8 Practical Realisation

A practical realization of the Extended 6 DoF Abbe comparator principle is shown in Figure 98.

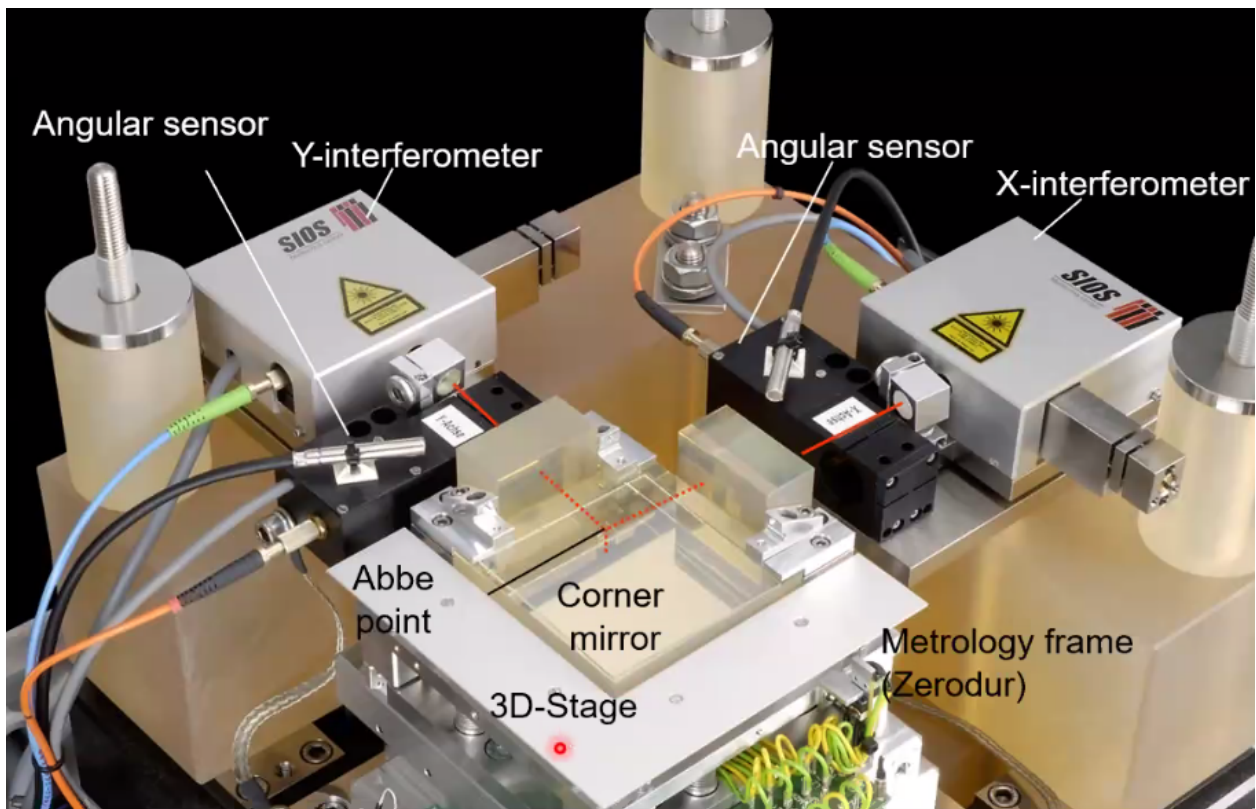


Figure 98: Practical Realization of the

## 8.9 Tilt Compensation

To measure compensate for any tilt, two solutions are proposed:

1. Use a zero point angular auto-collimator (Figure 99)
  - Resolution: 0.005 arcsec
  - Stability (1h): < 0.05 arcsec
2. 6 DoF laser interferometer (Figure 100)
  - Resolution: 0.00002 arcsec
  - Stability (1h): < 0.00005 arcsec

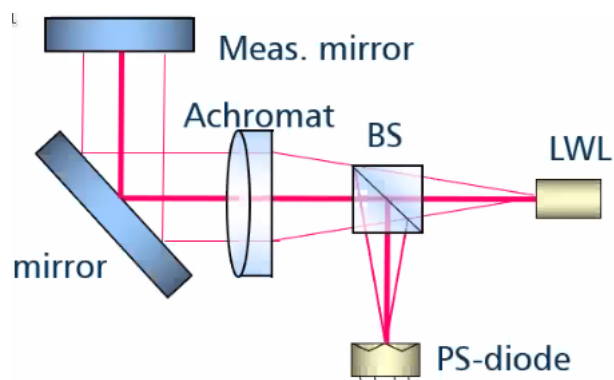


Figure 99: Auto-Collimator

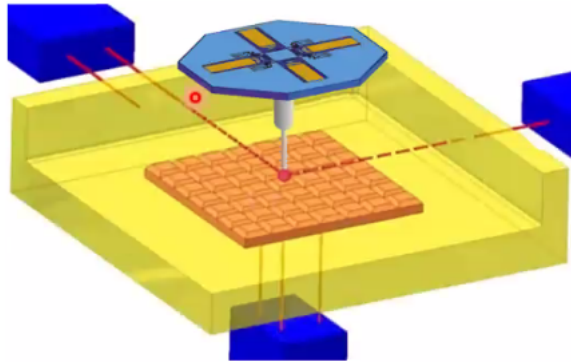


Figure 100: 6 Interferometers to measure tilts

## 8.10 Comparison of long travel guiding systems - Bis

Now, if we actively compensate the tilts are shown previously, we can fulfill the requirements as shown in Figure 101.

Measurement and control technology to minimize Abbe errors to achieve:

- sub-nanometer precision
- smaller moving mass
- better dynamics

	air bearing	precision roller bearing	precision roller bearing + meas. & control
moving mass	large	smaller	smaller
dynamics	limited	better	better
effort	expensive	moderately	more complex
angular deviation	2 arcsec.	20 arcsec.	< 0.05 arcsec.
Abbe error ( $l_{\text{off}}=200 \mu\text{m}$ )	2 nm	20 nm	< 0.05 nm
Requirement: < 1 arcsec.	technically not feasible		yes

Figure 101: Characteristics of the tilt compensation system

## 8.11 Drive concept

Usually, in order to achieve a large range over small resolution, each axis of motion is a combination of a coarse motion and a fine motion stage. The coarse motion stage generally consist of a stepper motor while the fine motion is a piezoelectric actuator.

The approach here is to use an **homogenous drive concept for increase dynamics** (Figure 102).

Only one linear voice coil actuator is used which with large moving range and sub-nanometer resolution can be achieve at one time.

## 8.12 NPMM-200 with extended measuring volume

The NPMM-200 machine can be seen in Figure 103.

Characteristics:



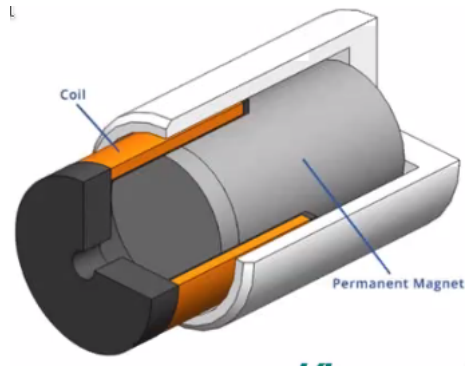


Figure 102: Voice Coil Actuator

- Measuring range: 200 mm x 200 mm x 25 mm
- Resolution: 20 pm
- Abbe comparator principle
- 6 laser interferometers
- Active angular compensation
- Position uncertainty < 4 nm
- Measuring uncertainty up to 30 nm

The NPMM-200 actually operates inside a Vacuum chamber as shown in Figure 104.

### 8.13 measurement capability

Some step responses are shown in Figure 105 and show the nano-metric precision of the machine. Picometer steps can even be achieved as shown in Figure 106.

### 8.14 Extension of the measuring range (700mm)

If the measuring range is to be increase, there are some limits of the moving stage principle:

- large moving masses ( $\sim 300\text{kg}$ )
- powerful drive systems required
- nano-meter position capability problematic
- large heat dissipation in the system
- dynamics and dynamic deformation

The proposed solution is to use **inverse dynamic concept for minimization of moving masses.**

### 8.15 Inverse kinematic concept - Tetrahedral concept

The proposed concept is shown in Figure 107:

- mirrors and object to be measured are fixed
- probe and interferometer heads are moved
- laser beams virtually intersect in the probe tip

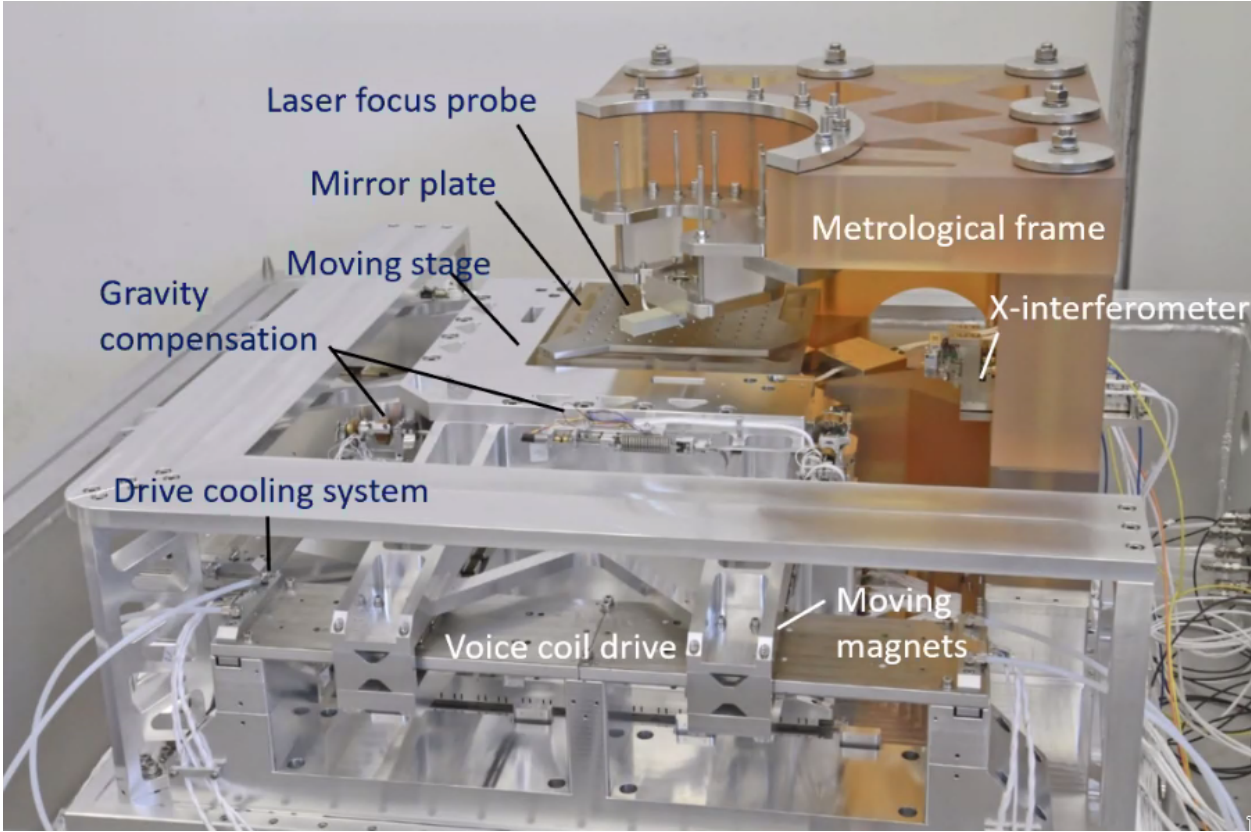


Figure 103: Picture of the NPMM-200

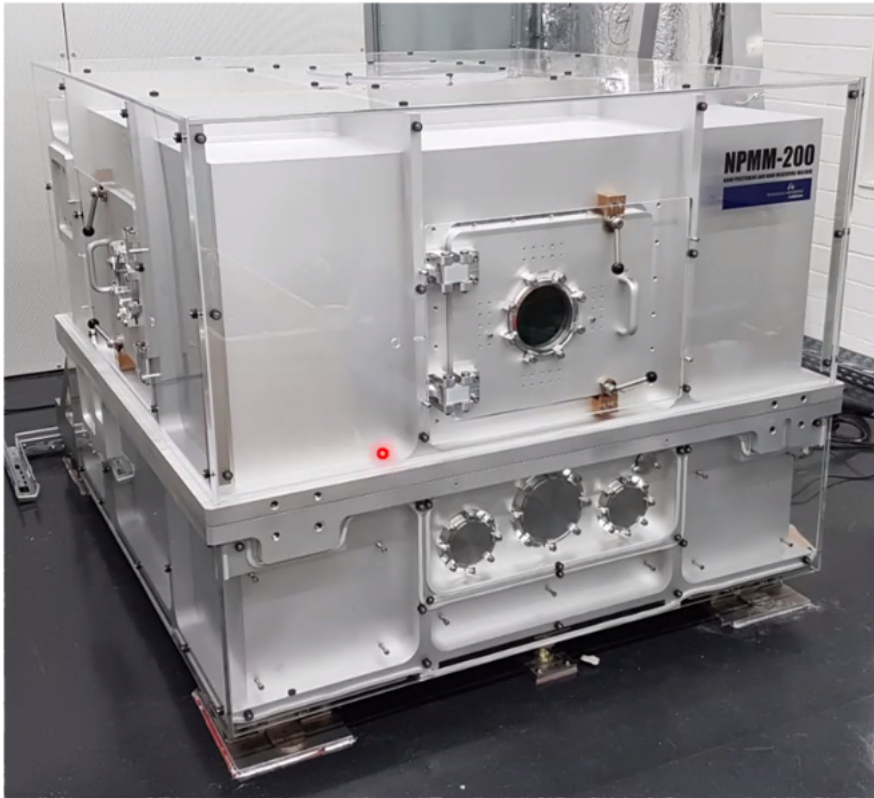


Figure 104: Vacuum chamber used

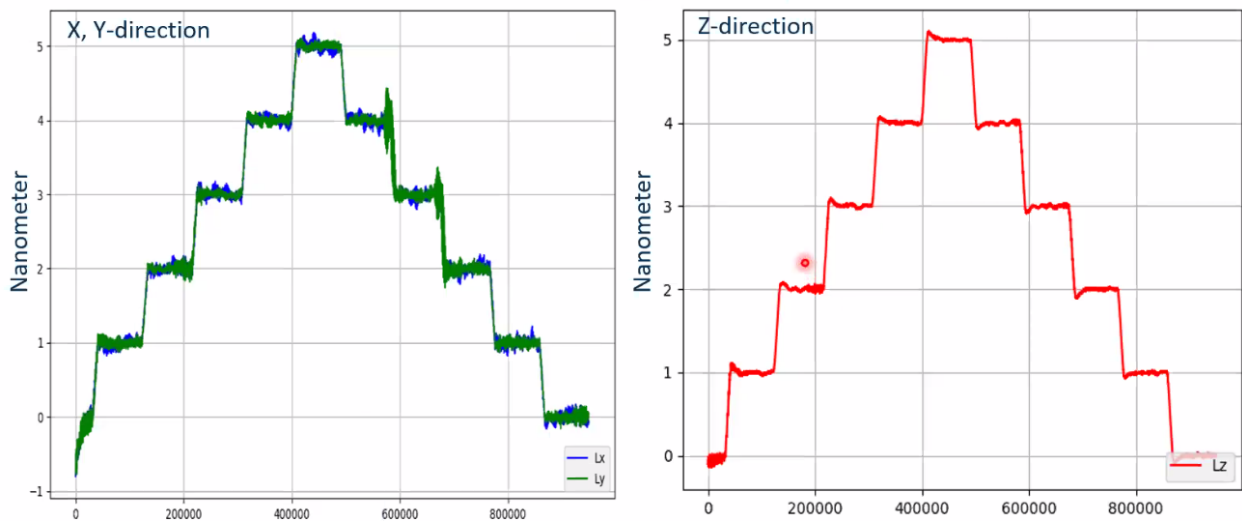


Figure 105: Sub nano-meter position accuracy

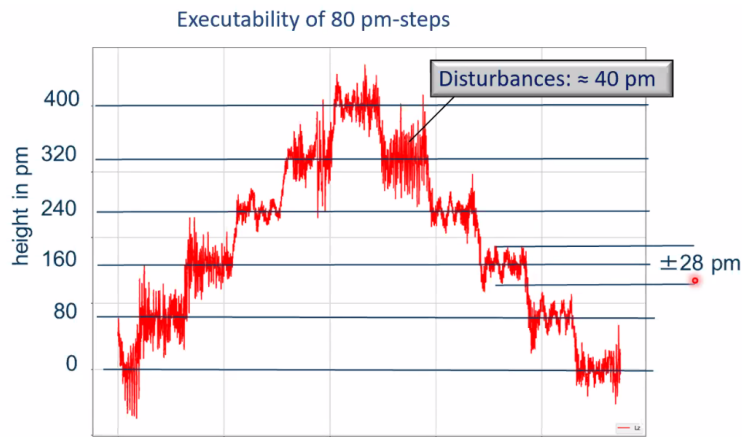


Figure 106: Picometer level control

- Tetrahedral measuring volume

This fulfills the Abbe principle but:

- large construction space
- difficult guide and drive concept

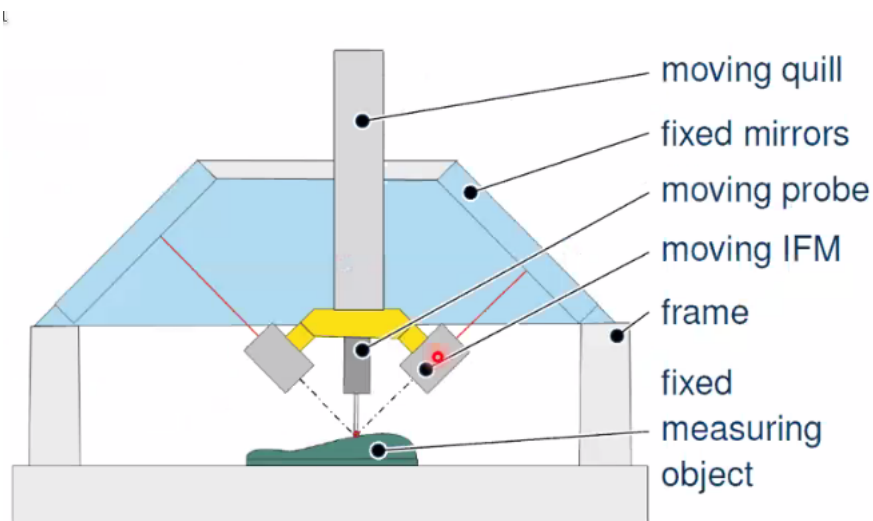


Figure 107: Tetrahedral concept

### 8.16 Inverse kinematic concept - Scanning probe principle

An other concept, the scanning probe principle is shown in Figure 108:

- cuboidal measuring volume
- Fixed x-y-z mirrors
- moving measuring head
- guide and drive system outside measuring volume

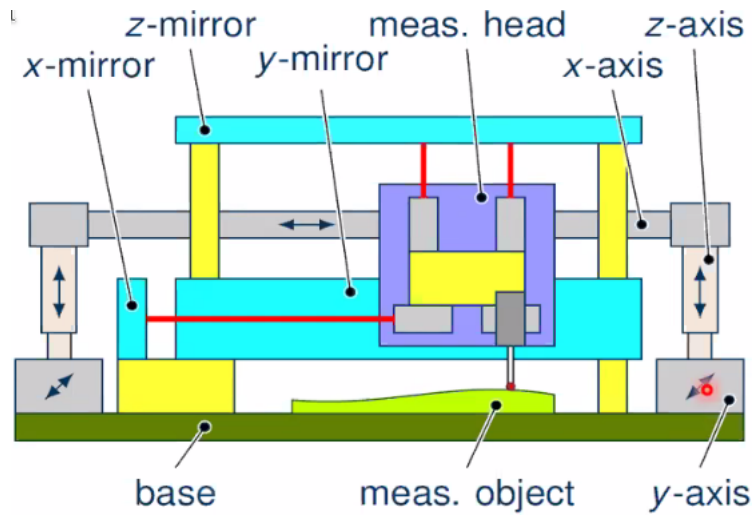


Figure 108: Scanning probe principle

### 8.17 Inverse kinematic concept - Compact measuring head

In order to minimize the moving mass, compact measuring heads have been developed. The goal was to make a lightweight measuring head (<1kg)

The interferometer used are fiber coupled laser interferometers with a mass of 37g (Figure 109).

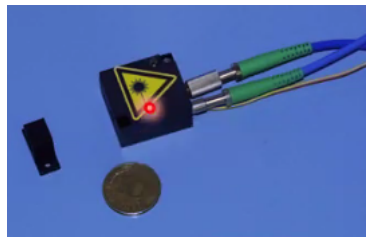


Figure 109: Micro Interferometers

The concept is shown in Figure 8.17:

- 6dof interferometers are used
- one micro-probe
- the total mass of the head is less than 1kg

There is some abbe offset between measurement axis of probe and of interferometer but **Abbe error compensation by closed loop control of angular deviations** is used.

### 8.18 Inverse kinematic concept - Scanning probe principle

As shown in Figure 110, the abbe error can be compensated from the two top interferometers as:

$$\text{for } l_x = a : \quad \Delta l_{\text{Abbe}} = \Delta l_{\text{int}}$$

Thus the tilt and Abbe errors can be compensated for with sub-nm resolution.

### 8.19 Conclusion

Proposed approaches to push the nano-positioning and nano-measuring technology:

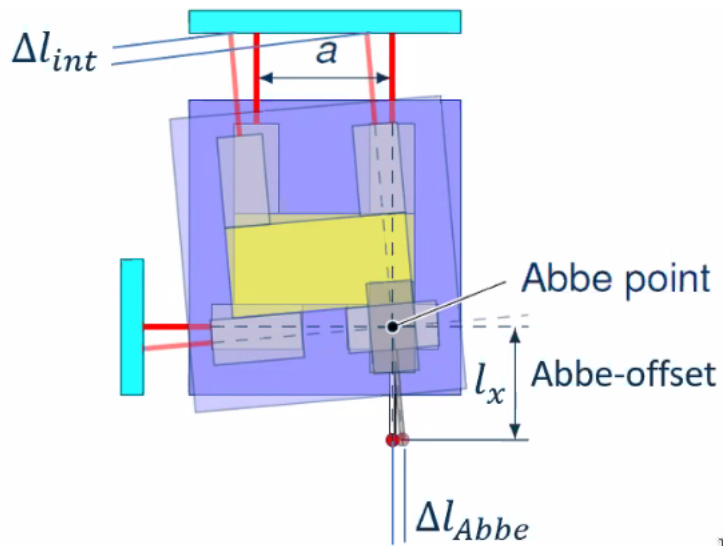
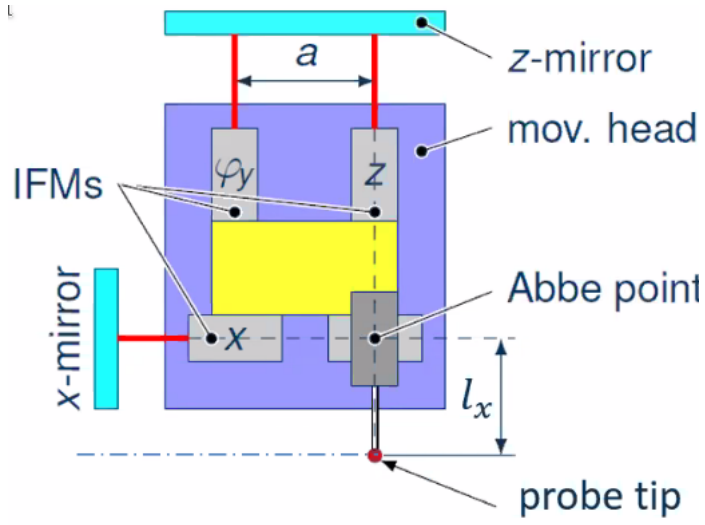


Figure 110: Use of the interferometers to compensate for the Abbe errors

- Measurement and control technology to minimize Abbe errors
- Homogeneous drive concept for increased dynamics
- Inverse kinematic concept for minimization of moving mass
- Abbe-error compensation by closed loop control of angular deviations

## 9 Reducing control delay times to enhance dynamic stiffness of magnetic bearings @jan\_philipp\_schmidtman

### 9.1 Introduction

This project focuses on reducing the control delay times of a magnetic bearing shown in Figure 111.

- For a novel printing process, 6-DOF positioning with a long linear stroke is required
- Conventional linear guides provide only 1-DOF



Linear actuator (1-DOF) with magnetic guide (5-DOF) allows combined 6-DOF positioning

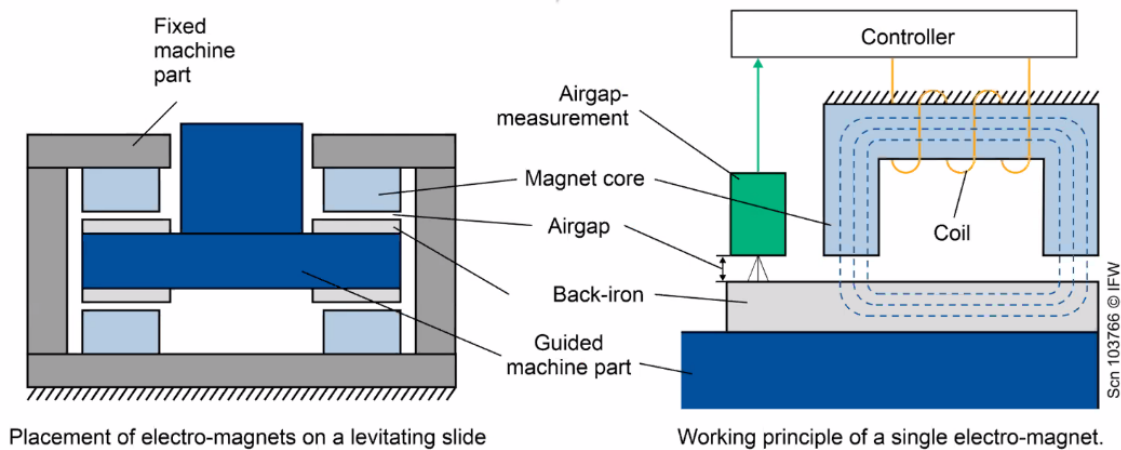


Figure 111: 6 DoF Position System - Concept

Active magnetic bearings are unstable systems and require active control. However, the active control of magnet forces leads to a control delay that limits the performances (stiffness) of the bearing.

### 9.2 Time Delay Reduction

Typical contributors to the control delay time are shown in Figure 112.

The reduction of the control time delay will increase the dynamic stiffness of the bearing as well as decrease the effects of external disturbances and hence improve the positioning errors (Figure 113).

The steps to reduce the control delay time are:

1. Eliminate BUSS-communication by merging position and current controller
2. Reduce cycle time by using rapid prototyping system
3. Reduce delay in PWM driver by using high PWM frequencies with SiC driver

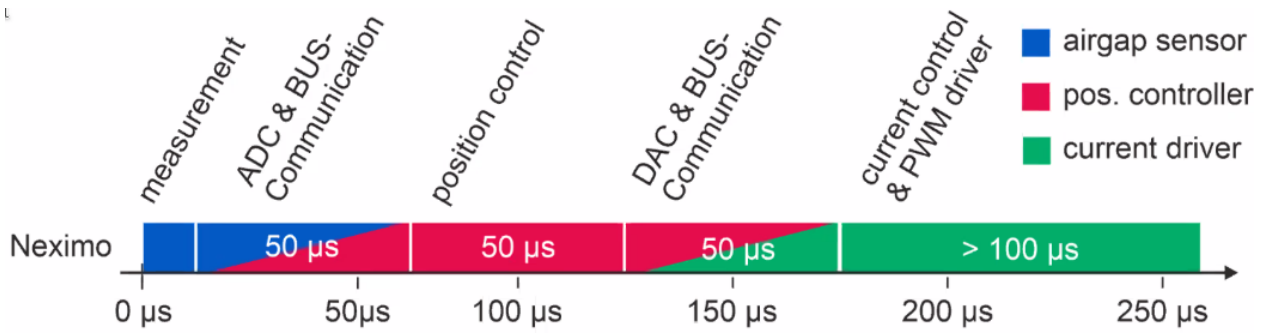


Figure 112: Typical Contributors to control delay time

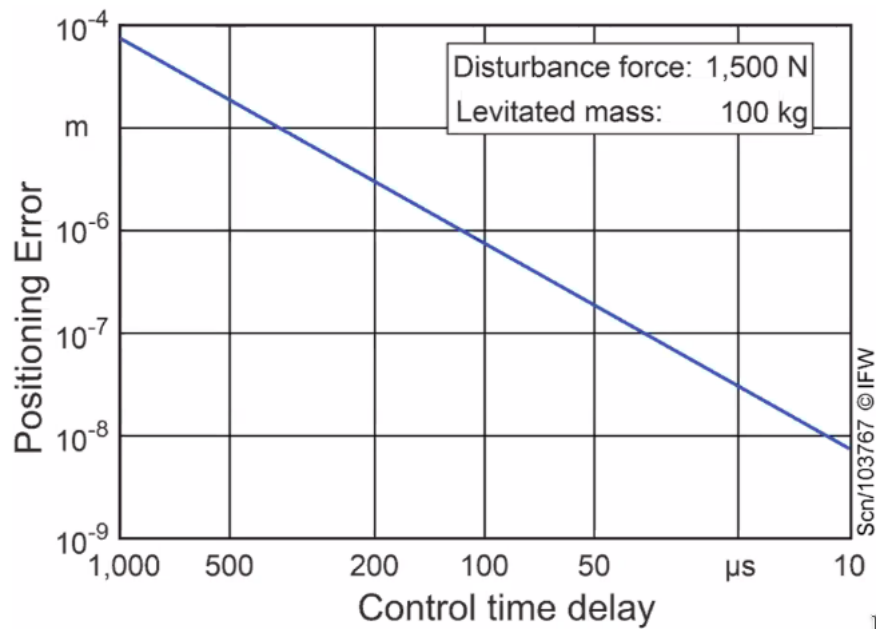


Figure 113: The effect of control delay on stiffness



Figure 114: Controller for position and current



### 9.3 Practical Realization

Therefore, the position and current control have been merged into one controller (Figure 114).

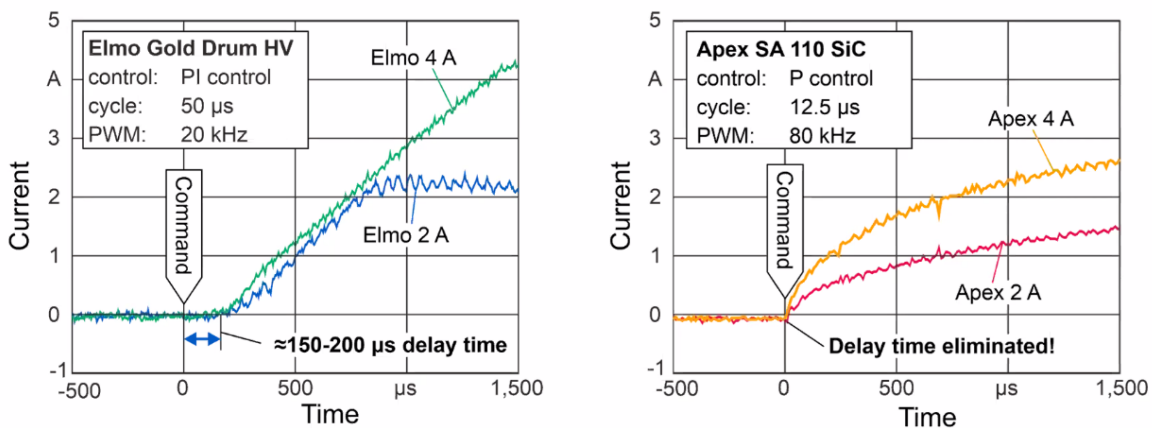
A dSpace rapid prototyping system is used for fast position and current control. Characteristics of the used elements are shown in Figure 115.

Current driver		Control Systems	
Type	APEX SA 110 SiC half bridge driver	Type	dSpace DS1103
PCB Layout	Modified APEX Evaluation Kit 43	PWM out	80 kHz
PWM frequency	< 400 kHz	Cycle time	12.5 μs
Current	< 28 A	<b>Current sensing</b> Type      INA 282 current shunt monitor	
Voltage	< 400 V		

Figure 115: Setup for reduced delay times

### 9.4 Results

Differences between the previous PWM controller and the new SiC controller are shown in Figure 116. The delay time is almost completely eliminated.



**Current measurement:**  
 scope: Agilent MS06014A  
 sensor: Chauvin Arnoux E3N 100 mV/A

**Magnet:**  
 windings: 100      core: E-core  
 rated/ max. current: 6 A / 20 A      airgap: 0.5 mm  
 resistance: 0.15 Ω

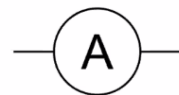


Figure 116: Reduction of delay in PWM Driver

### 9.5 Conclusion

Due to all the performed modifications, the control delay time could be reduced by 80%. The next steps for this project are shown in Figure 117.

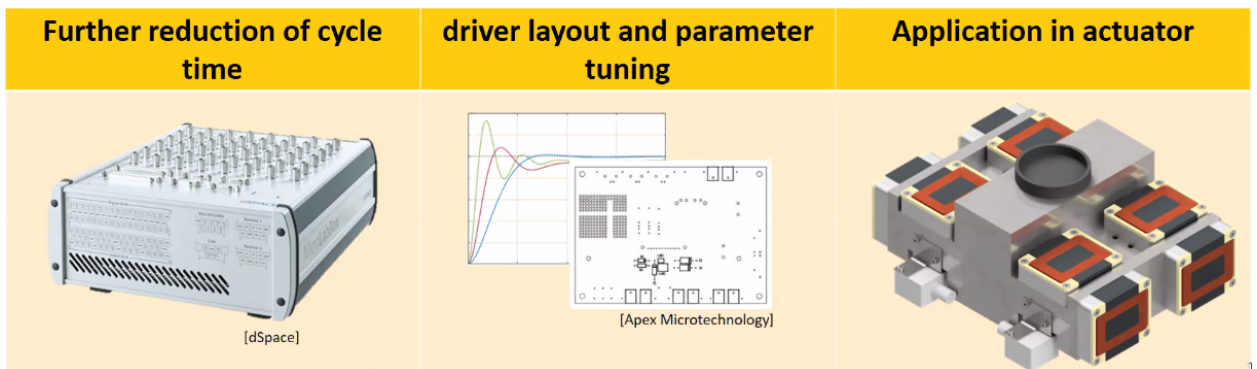


Figure 117: Next Steps

## 10 Digital twins in control: From fault detection to predictive maintenance in precision mechatronics @koen\_classens

### 10.1 Motivation

Models are usually for the control design part that can be either physical models (FEM, first principle) or data-driven models. However, these models are usually not used after control system is implemented (Figure 118).

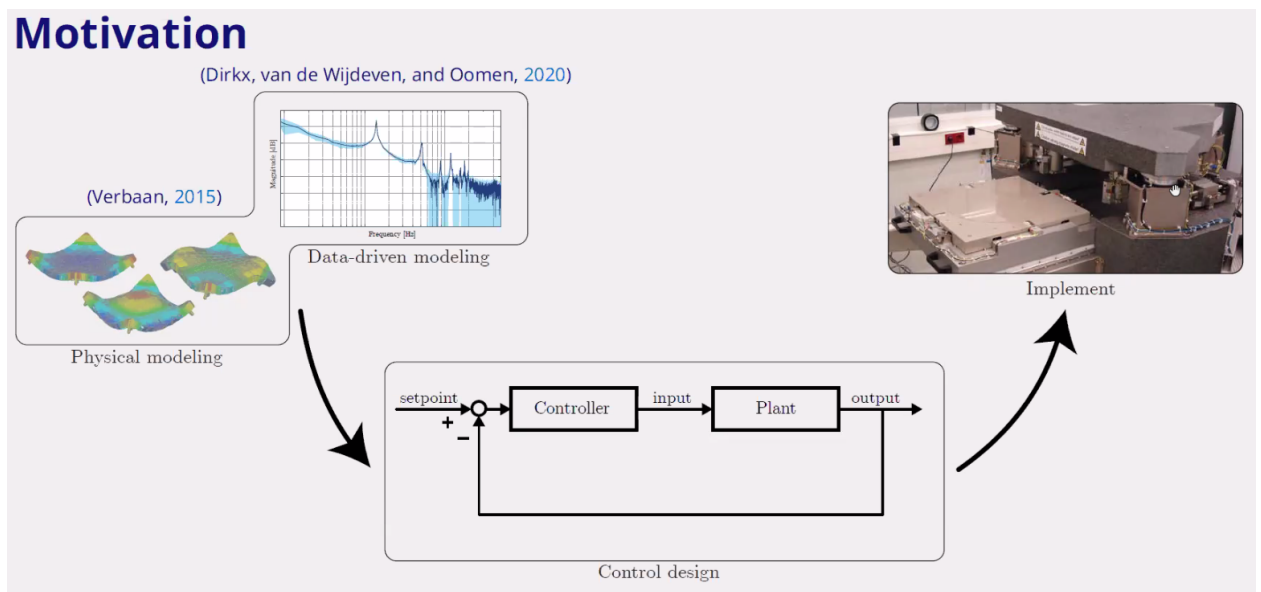


Figure 118: Typical of of models in a mechatronic system

Here, the models are exploited to monitor the system and predict future possible failures in the system. Use models as digital twin for **fault detection and Isolation for predictive maintenance in precision mechatronics** (Figure 119).

### 10.2 Predictive Maintenance

Classical maintenance happens when the system is not working anymore as shown in Figure 120.

It is possible to perform some preventive maintenance before a failure happens, but this is still not optimal.

The idea here is to predict when the failure will happen in order to only do maintenance only when really necessary. This will minimize the down time of the machine.

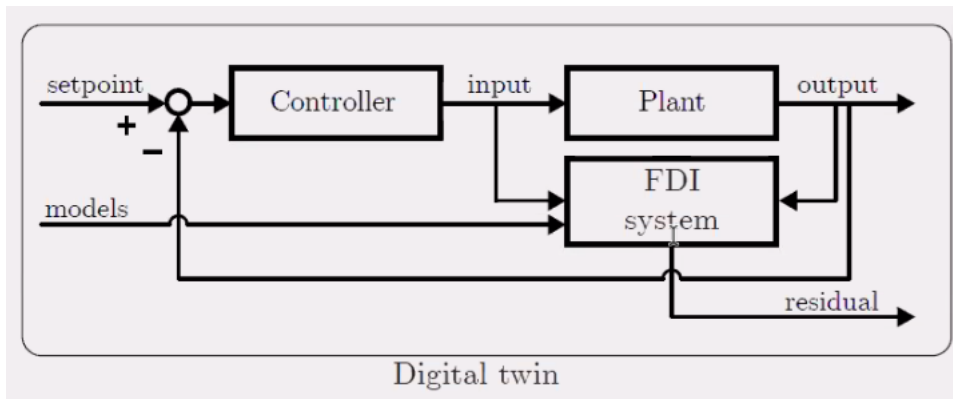


Figure 119: FDI is using the model of the plant

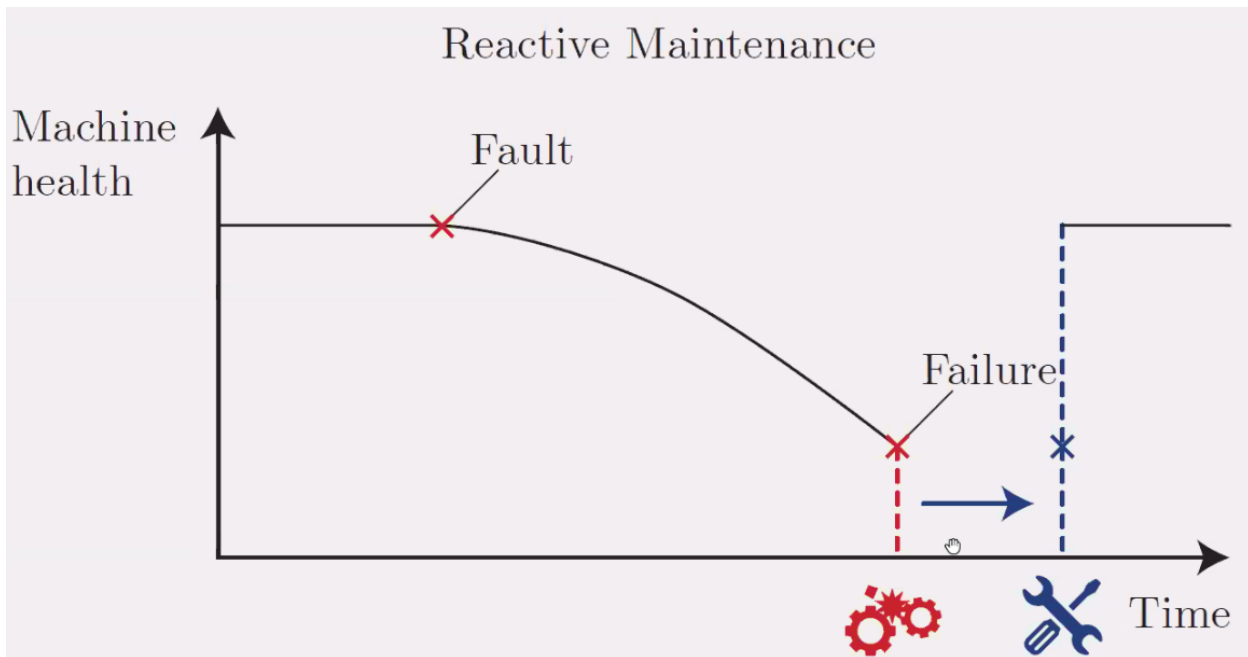


Figure 120: Maintenance done when a failure is appearing

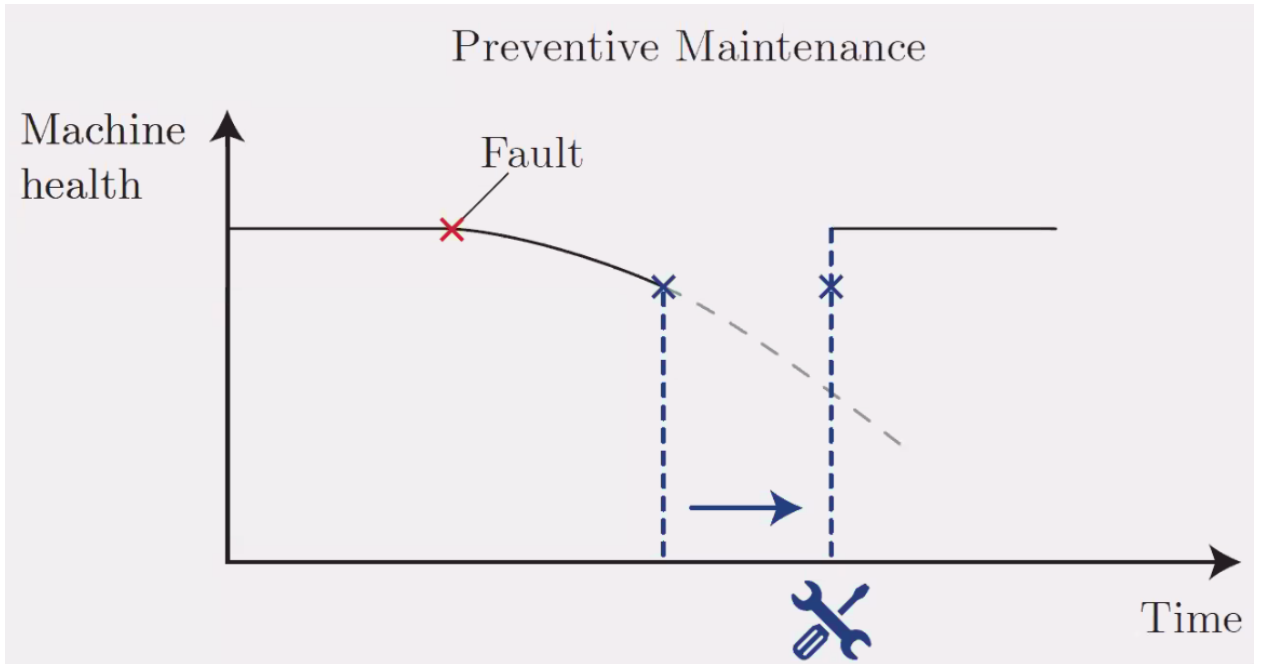


Figure 121: Preventive Maintenance

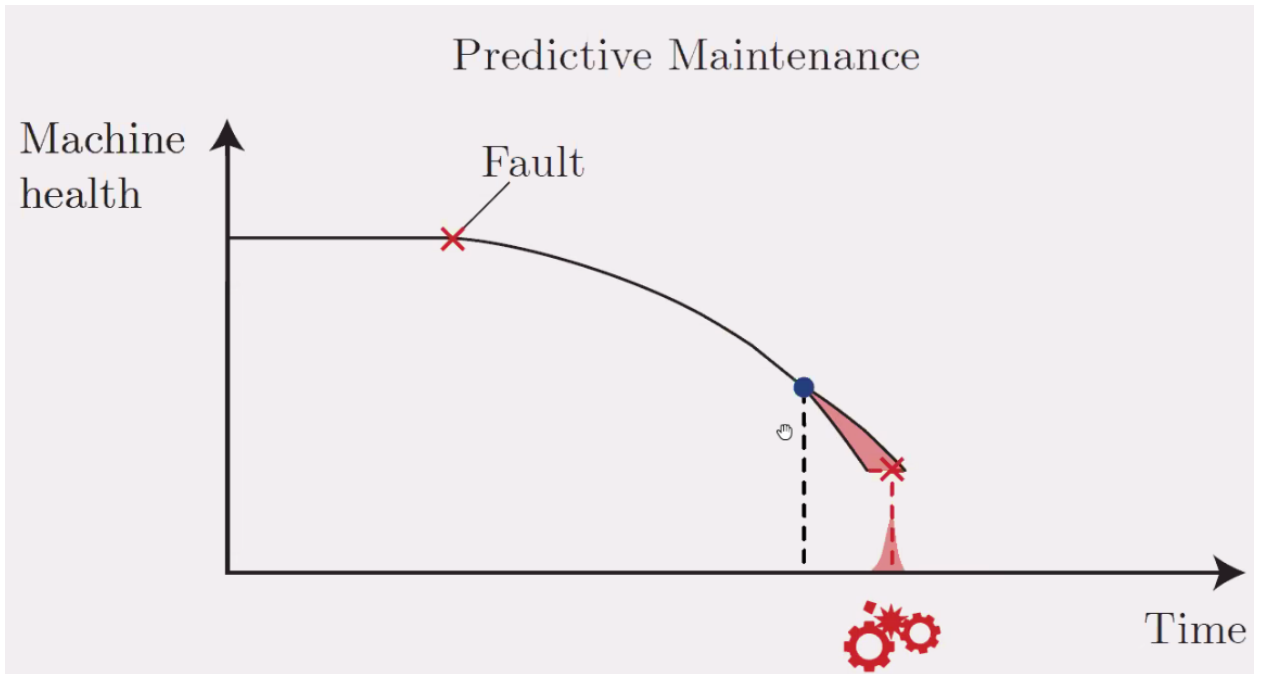


Figure 122: Predictive maintenance

### 10.3 Objectives

The main objective is to develop a system monitoring approach for precision mechatronic systems, exploiting prior information (models) and integrating posterior information (real-time measured data).

Even though state of the art system monitoring are already in used in aerospace, process industry and automotive, there are few specificity for mechatronic systems:

- Control loops
- Large-scale MIMO systems (interaction)
- Accurate models: Frequency Response Functions

### 10.4 Null-space based FDI

The goal is to applied a decentralized Fault Detection on the system shown in Figure 123 to detect actuator faults at  $J_1$ . This should take into account the control loop, interaction in the system and be FRF based.

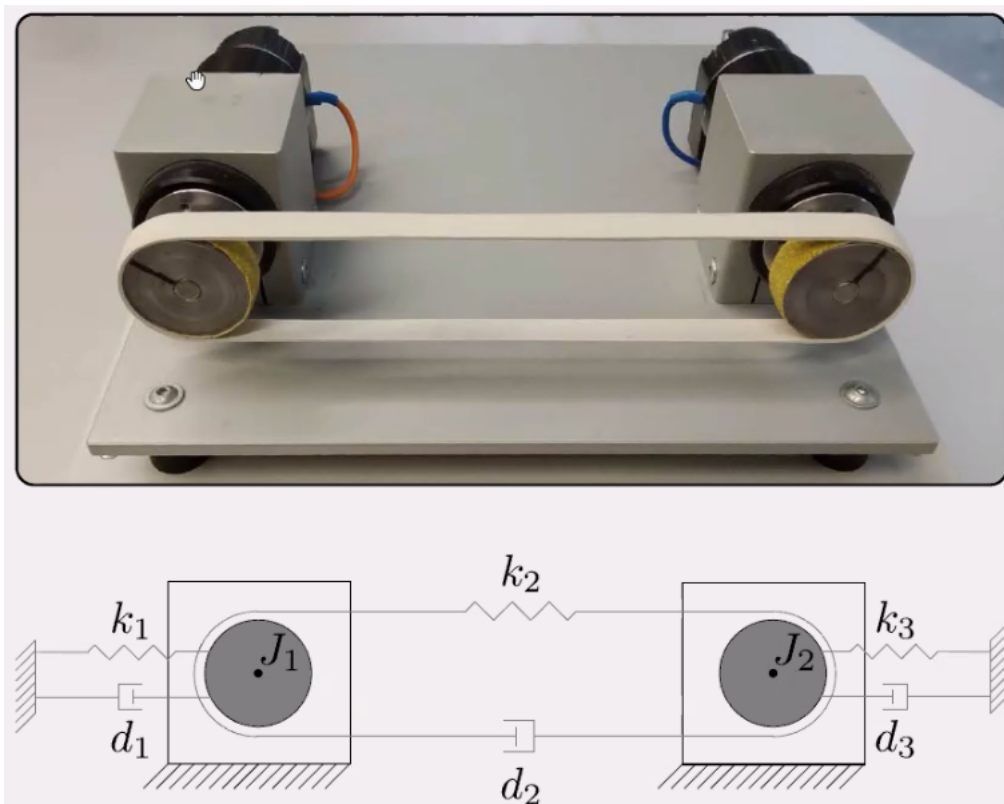


Figure 123: Test System

The architecture to estimate faults in the system is shown in Figure 124. The goal is to design  $Q_u$  and  $Q_y$  such that  $\epsilon$  is a representation of faults in the system.

When a fault happens (Figure 125), the outputs signals are not changing that much (because of feedback), however the system is able to find that there is a problem using the residual  $\epsilon$ .

**Procedure:**

- Additive faults
- Closed-loop
- Interaction
- start from identification

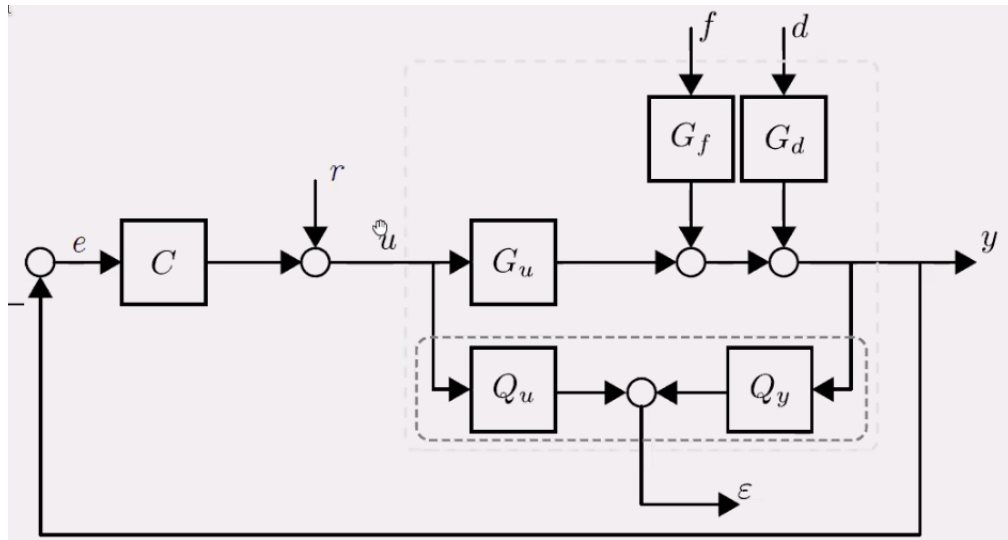


Figure 124: Residual Generator

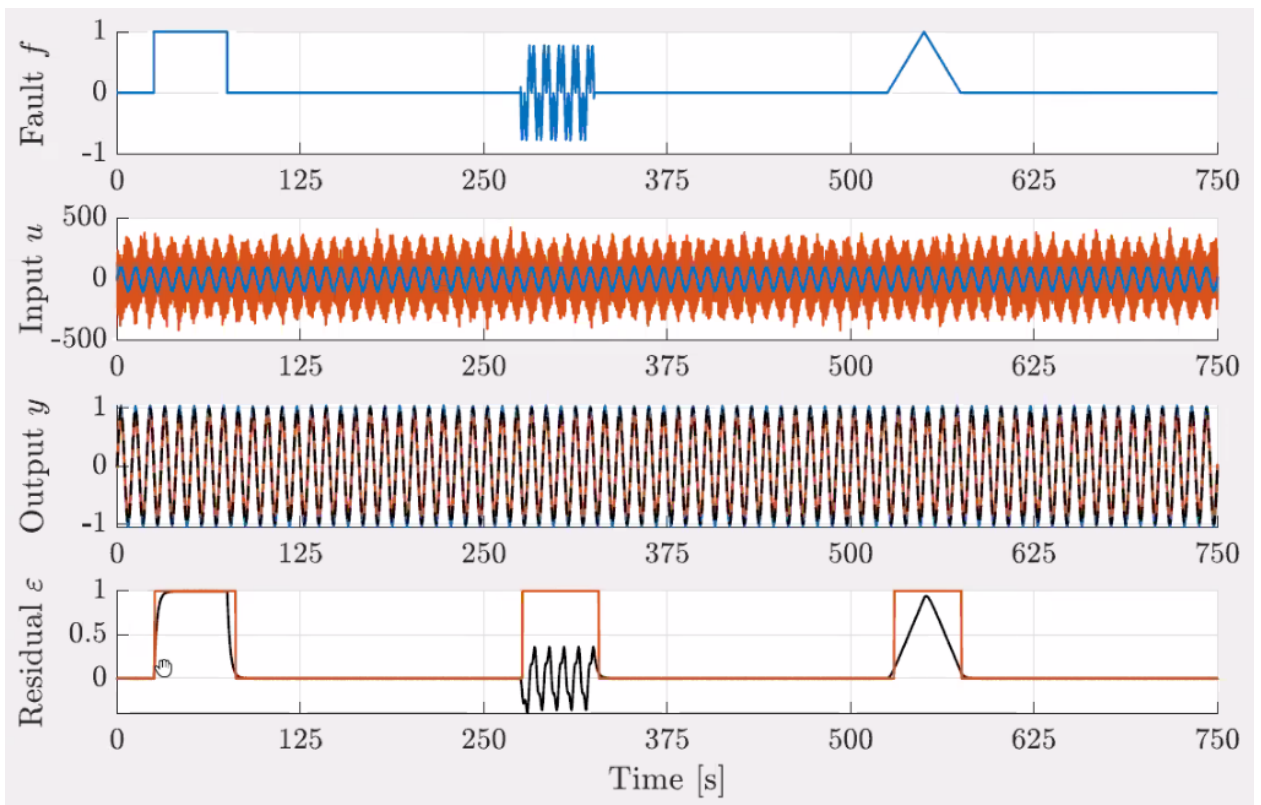


Figure 125: Simulation Results

## 10.5 Roadmap from fault detection to predictive maintenance

The proposed system can detect faults in the system (Figure 126). This proof of principle should now be applied on industrial systems. Moreover, from the fault detection, predictive maintenance should be performed (Figure 126).

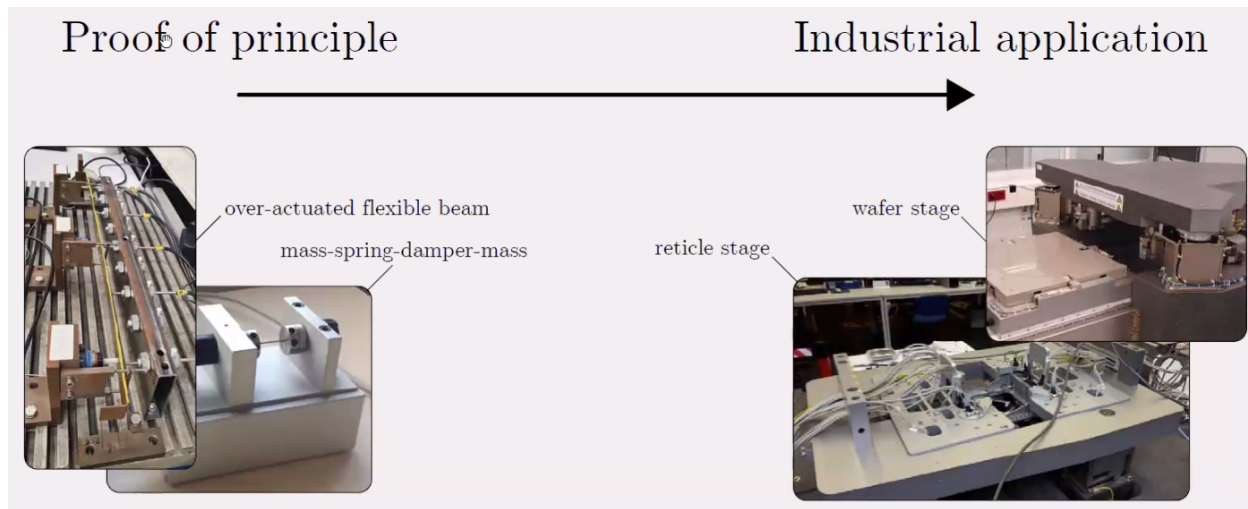


Figure 126: From proof of principle to industrial application

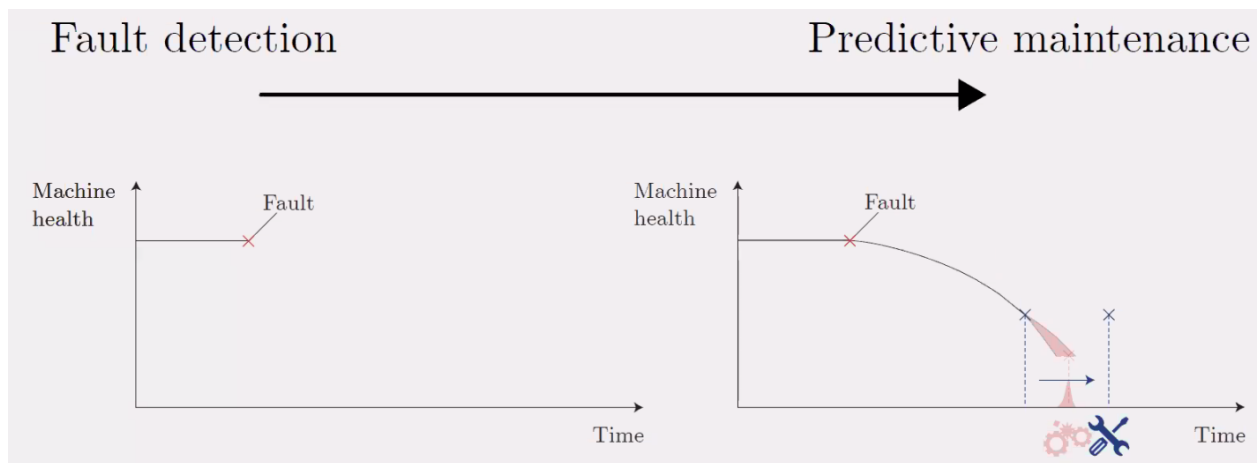


Figure 127: From fault detection to predictive maintenance